Received June 15, 2017, accepted June 30, 2017, date of publication July 5, 2017, date of current version August 8, 2017.

Digital Object Identifier 10.1109/ACCESS.2017.2723822

On Spectral Coexistence of CP-OFDM and FB-MC Waveforms in 5G Networks

QUENTIN BODINIER, (Student Member, IEEE), FAOUZI BADER, (Senior Member, IEEE), AND JACQUES PALICOT, (Member, IEEE)
SCEE Research Team, CentraleSupélec/IETR, 35576 Rennes, France

Corresponding author: Quentin Bodinier (quentin.bodinier@supelec.fr)

This work was supported in part by the French National Research Agency projects ACCENT5 under Grant ANR-14-CE28-0026-02 and EPHYL under Grant ANR-16-CE25-0002-03.

ABSTRACT Future 5G networks will serve a variety of applications that will coexist on the same spectral band and geographical area in an uncoordinated and asynchronous manner. It is widely accepted that using cyclic prefix-orthogonal frequency division multiplexing (CP-OFDM), the waveform used by most current communication systems, will make it difficult to achieve this paradigm. Especially, CP-OFDM is not adapted for spectral coexistence because of its poor spectral localization. Therefore, it has been widely suggested to use filter bank-based multicarrier (FB-MC) waveforms with enhanced spectral localization to replace CP-OFDM. Especially, FB-MC waveforms are expected to facilitate coexistence with legacy CP-OFDM-based systems. However, this idea is based on the observation of the power spectral density of FB-MC waveforms only. In this paper, we demonstrate that this approach is flawed and show that interference between FB-MC and CP-OFDM systems should be rated on precise estimation of the error vector magnitude. Our analysis, which is confirmed through simulations on both flat and frequency selective channels and software radio implementation, shows that the interference caused by FB-MC waveforms on CP-OFDM receivers is multiple orders of magnitude higher than expected in the literature. Finally, our results show that using FB-MC waveforms does not facilitate coexistence with CP-OFDM-based systems to a high extent.

INDEX TERMS Coexistence, 5G, OFDM, filter banks, FBMC, OFDM/OQAM, GFDM, FMT, FBMC-PAM, COQAM, interference analysis.

I. INTRODUCTION

The advent of the 5th Generation of wireless communication systems (5G) is envisioned to bring flexibility to cellular networks. New services as Device-To-Device (D2D) or Machine-To-Machine (M2M) communications are already being progressively deployed. It is expected that the volume of these new communication types, catalyzed by the emergence of the Internet of Things (IoT), will grow exponentially in the coming years. The wireless world of tomorrow will therefore be holistically different from the centralized, homogeneous and synchronous cellular networks which abide by the current Long Term Evolution-Advanced (LTE-A) standards [1].

This new paradigm requires the physical layer (PHY) of 5G to be adaptable to various situations, and robust to asynchronous interference coming from neighboring communication devices [2], [3].

Besides, these new communication types will add a new burden to the radio spectrum, which is already saturated. To answer this challenge, two directions have mainly been explored:

1) Exploit new parts of the spectrum at higher frequencies above 6 GHz.
2) Exploit parts of the already licensed spectrum that are temporally left free by incumbent users.

Point (i), which is for example related to research on mm-wave communications, is out of the scope of this article. In this study, we rather focus on point (ii). The main challenge to overcome when re-exploiting some parts of the already licensed spectrum lies in the fact that the secondary users should insert their communication without causing harmful interference to the incumbent legacy users. In the context of 5G, a significant part of the reusable spectrum belongs to either LTE-A cellular networks, Wi-Fi, WiMAX or TV bands. In all these cases, inserted secondary users will have to coexist with CP-OFDM based incumbent communications, as it is the waveform used by these technologies. Note

that Single Carrier-Frequency Division Multiplexing Access (SC-FDMA) used in the uplink of cellular LTE-A communications is also based on the transmission of Fourier Spread CP-OFDM symbols.

Therefore, future devices deployed in the course of the development of 5G will likely coexist with CP-OFDM based systems. However, it is crucial that newly introduced services do not interfere in a harmful manner with incumbent legacy communications. This issue has been identified as one of the core challenges of cognitive radios by Haykin in [4], where the notion of ''interference temperature'' was introduced. Currently, to protect the incumbent CP-OFDM users, the common policy states that all users should respect a certain spectrum mask at the transmitter side. In other words, the Power Spectral Density (PSD) of transmitted signals must fit below certain limits specified by the standards. Because of the poor spectral containment of CP-OFDM, it is usually necessary to turn off an important amount of guard subcarriers to fit the specified masks, which incurs an important loss in terms of spectral efficiency. This is a major pitfall which makes coexistence between unsynchronized CP-OFDM systems hardly feasible.

Building on this observation, the research community has investigated the possibility to use new waveforms with improved spectral containment instead of CP-OFDM, so that the secondary transmissions of 5G systems could more easily fit into the spectrum masks specified by incumbent legacy CP-OFDM users. Most new waveform schemes proposed so far fall into the category of filter bank based multicarrier (FB-MC) waveforms. They all rely on filtering the transmit signal through highly frequency selective filters to reduce out-of-band (OOB) emissions. Therefore, users based on this type of waveform fit more easily the spectral masks set by incumbent users. Based on this observation, an important number of research works have investigated the potential gains obtained by using FB-MC waveforms for coexistence with CP-OFDM based users.

A. RELATED WORK

The first works related to coexistence of secondary users with CP-OFDM incumbent users date back to the beginning of the century. The cognitive radio concept increasingly gained popularity after Mitola's Ph.D. dissertation [5] and the need for a model of interference usable for cognitive radio deployments was soon identified in [4]. However, at this time, the research community did not identify clearly the links between this concept and the PHY layer problematics, especially the choice of waveform. It is only when Weiss and Jondral coined the term ''spectrum pooling'' in [6] that they defined a waveform-dependent model to compute interference between systems coexisting on the same spectral band. The model they defined went on to be known as the ''PSD-based model'' in the literature.

This model has then been extensively used to compute interference between secondary and incumbent users in cognitive radio scenarios in which both systems would utilize CP-OFDM [6], [7]. Because of the high OOB emissions of CP-OFDM, research works based on the PSD-based model showed that CP-OFDM is not well adapted for spectrum sharing between secondary and incumbent users [8]. This observation was one of the many arguments that fostered the research of a new waveform able to replace CP-OFDM in 5G systems.

All FB-MC multicarrier waveforms proposed to replace CP-OFDM rely on some filtering to improve the spectral localization of the emitted signals. Some of them perform a per-band filtering, meaning that groups of subcarriers are passed together through a filter. Among this group of subband-filtered waveforms, the two leading proposals are filtered-OFDM (f-OFDM) [9] and universal filtered OFDM (UF-OFDM) originally called universal filtered multi-carrier (UFMC) [10]. In this paper however, we are interested in subcarrier-filtered waveforms which perform, as their name indicates, a subcarrier-wise filtering on the transmitted signal so that each waveform is highly spectrally localized. Among these waveforms, we consider Filtered Multi-Tone (FMT), offset quadrature amplitude modulated-OFDM (OFDM/OQAM), FBMC with pulse amplitude modulation (FBMC-PAM), generalized frequency division multiplexing (GFDM) and FBMC/circular OQAM(COQAM). [11]–[18]

In FMT modulation [11], [12], a guard band is added between every subcarrier so that they do not overlap. Therefore, FMT suffers from some bandwidth efficiency loss. To increase spectral efficiency, OFDM/OQAM [13], [14] allows for adjacent subcarriers to overlap. Unlike FMT, real symbols modulated according to a PAM constellation are transmitted on each subcarrier. A $\frac{\pi}{2}$ phase difference is applied to adjacent subcarriers, which provides real-domain orthogonality. However, OFDM/OQAM requires doubling the symbol rate. To avoid that, FBMC-PAM modulation has been recently proposed by Bellanger *et al.* in [15]. In this scheme, the number of subcarriers is doubled instead of the number of time symbols. A drawback common to all the aforementioned modulations is the transient imposed by their transmit and receive filters. GFDM tackles this problem by application of cyclic pulse shaping [16]. However, this comes at the expense of higher OOB emissions, which is due do the discontinuities induced in the signal by truncation in time with a rectangular window [17]. Finally, COQAM consists in a mix between GFDM and OFDM/OQAM [18]: OQAM symbols are transmitted through a set of circular filter banks.

Whatever the specific details of the aforementioned waveforms, they all achieve lower OOB emissions than CP-OFDM thanks to their inherent filtering of the transmitted symbols. Because of these advantageous PSD properties, an important amount of research works have investigated the benefits of using these FB-MC waveforms for coexistence with legacy CP-OFDM incumbent users, for example [7], [19]–[22]. Interestingly, to rate interference between coexisting systems, many of these studies applied the PSD-based model in heterogeneous scenarios in which the secondary and incumbent

systems do not use the same waveform, even though this model was originally designed to analyze scenarios in which both systems use CP-OFDM.

Aforementioned studies built on the PSD-based model predicted that it would be very efficient to use FB-MC waveforms to coexist with CP-OFDM users. Because of these encouraging results, a number of real-world demonstrations of coexistence between FB-MC waveforms and CP-OFDM have also been undertaken by both industrials and academics [23]–[25]. In [23], the error vector magnitude (EVM) of the incumbent CP-OFDM receiver is studied, but the achieved values are not compared for multiple secondary waveforms. Therefore, this experiment does not enable us to rate the potential gains of using FB-MC for coexistence. Kaltenberger *et al.* [24] and [25] measure experimentally the layer 3 goodput of a LTE uplink receiver confronted with interference coming from an asynchronous secondary transmitter. They show that if the latter uses GFDM, it can transmit approximately with 3 dB more power than a secondary that would use OFDM. Though this is an interesting gain, it is fairly less significant than what would be expected with the PSD-based model. Berg *et al.* [26] study the coexistence of a secondary OFDM/OQAM system with a TV receiver and show that it could transmit with 9 dB more power than a CP-OFDM secondary system without destroying the TV signal. Once again, this gap seems interesting but is not in line with results obtained with the PSD-based model for example in [7] in which it is predicted that FB-MC systems can be assigned almost arbitrary high power without interfering on the primary if just one guard subcarrier is used. In this paper, we will therefore present in section VII an experiment that allows us to study the coexistence between a FB-MC and an OFDM systems in more details than those presented in [23]–[26] and, to the best of our knowledge, all other demonstrations available in the literature on the topic.

Overall, these experiments rely on high-level and sometimes qualitative metrics which encompass many effects and do not provide reproducible analysis. Moreover, they do not seem to be consistent with the PSD-based approach. Therefore, this shows that referring to the PSD of the secondary signal to compute interference in heterogeneous scenarios is not sufficient and a novel approach is needed. Moreover, the limitations of the PSD-based model, even in homogeneous scenarios, have been shown by Medjahdi *et al.* in [27]. However, to the best of our knowledge, only few research works have tackled the problem of coexistence between systems with different waveforms in an alternative manner. Most recently, Ahmed *et al.* [28] have analyzed the coexistence between UF-OFDM and CP-OFDM systems, but did not compare the results obtained when the secondary system uses UF-OFDM with those obtained if it was using CP-OFDM. In this article, we will also build upon some of our previous works, in particular [29]–[31]. In [29], we first remarked that the interference from FB-MC waveforms to CP-OFDM receivers was higher than expected through simulations, but this was not the core contribution of the work and only appeared as a side result. In [30] and [31], we focused on the coexistence of one particular FB-MC waveform, OFDM/OQAM, with CP-OFDM: in [30] we explained qualitatively the shortcomings of the PSD-based model, and in [31] we derived a theoretical analysis of the interference created by OFDM/OQAM onto CP-OFDM.

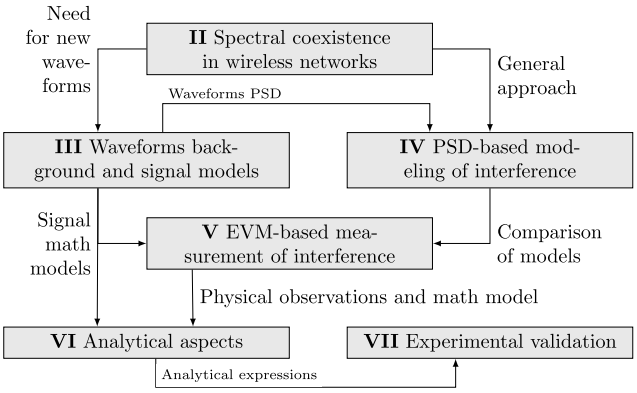

FIGURE 1. Organization of our analysis.

B. CONTRIBUTIONS

Based on the above review of the state of the art, the conclusion is clear: even though the research community has been extensively studying coexistence between FB-MC waveforms and CP-OFDM with both simulation and experimental approaches, there is still no accurate analytical model of interference available in the literature to study these scenarios, with the exception of the work in [28] for UF-OFDM and ours in [31] for OFDM/OQAM. Moreover, it has been noted that precise analysis of coexistence between CP-OFDM and FB-MC waveforms is an open issue that is important for various fields of research and that needs to be addressed [32]. We therefore propose to fill this gap in this article by accurately analyzing the interference between any FB-MC waveform and CP-OFDM in spectral coexistence scenarios. More precisely, in our discussion, we point out that looking at the PSD of the interfering signal is not sufficient because it does not encompass the operations performed by the receiver, as PSD is measured before the input antenna of the receiver that suffers from interference. We recall that interference should be measured after the receiver operations, based on EVM measurement. The contributions of the present article are five-fold:

1) We invalidate the PSD-based model and the results based on it for the analysis of scenarios in which systems based on different waveforms coexist.
2) We provide an analytical framework which explains why FB-MC waveforms do not significantly improve coexistence with CP-OFDM.
3) We devise analytical expressions of the interference caused by different FB-MC schemes on CP-OFDM and validate them through simulations.
4) We extend our analysis to multipath channels and evaluate the effects of FB-MC interference on the equal-

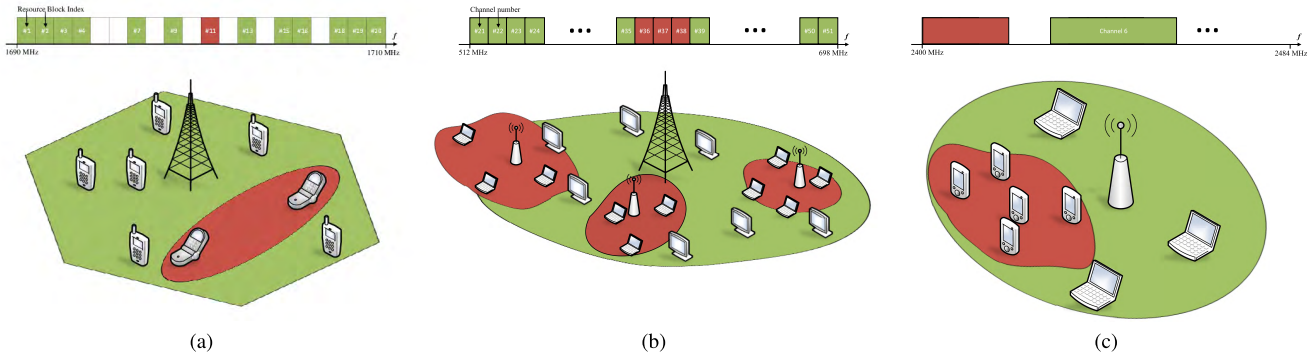

FIGURE 2. Examples of scenarios where the analysis of this article is relevant: (a) Insertion of an autonomous D2D link in a free resource block in the uplink band of a LTE cellular network. (b) Establishment of WLAN cells in TV white spaces. (c) Coexistence of ad-hoc mesh network with a Wi-Fi access point.

ization procedures that are performed at the incumbent CP-OFDM receiver.

5) We present a software radio testbed which is, to the best of our knowledge, the only currently existing experimentation platform that can analyze coexistence between FB-MC and CP-OFDM systems with the level of accuracy we provide. Furthermore, we show that experimental results perfectly validate our analysis.

This article is organized as described in Fig. 1: in section II, we present the idea of spectral coexistence in wireless networks, how it is usually tackled in the literature and the system model we propose to study it. Based on this, we explain why new waveforms have been sought, and we present the different waveform schemes we consider in section III. In Section IV we detail the PSD-based model that is commonly used to study those scenarios and show how it applies to the waveforms we consider. In section V, we propose a new measure to rate interference with more accuracy in coexistence scenarios. In section VI, we derive analytical expressions of interference according to the newly proposed model, and we validate the latter through an experiment that we present in sectionVII. Finally, section VIII concludes this article.

Notations: Scalars are noted x, vectors are bold-faced as $\mathbf{x}$ and sets are written with calligraphic letters $\mathcal{X}$. t represents continuous time, whereas m and n index respectively the subcarriers and the time slots. $\{.\}^*$ represent the complex conjugate, and $E_x\{y\}$ represents the expected value of y with respect to random variable x. Besides, $\overline{\mathbf{x}}$ represents the average value of vector $\mathbf{x}$. Finally $\star$ is the convolution operator.

II. SPECTRAL COEXISTENCE IN WIRELESS NETWORKS

A. SPECTRAL COEXISTENCE: DEFINITION

Coexistence in wireless networks is a notion that can take many meanings and forms; therefore, we feel that it is important to introduce our discussion by stressing out what **we** mean by spectral coexistence in wireless networks. For example, there has recently been a soaring interest for coexistence between Wi-Fi and LTE-M. This coexistence is enabled at the medium access control (MAC) layer through listen before talk procedures. This is **not** the type of coexistence that we are considering in this article.

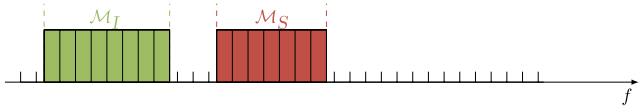

FIGURE 3. Spectral representation of the considered scenario. The incumbent and secondary systems coexist in the same spectral band, and each one is assigned a different subset of subcarriers.

Rather, the type of coexistence we cover in this work is similar to what was called "spectrum pooling" in the past [6], in which two systems coexist in the same spectral band, and each of them is assigned a specific part of the said band. An important assumption in our work is that the two coexisting systems operate independently, with no synchronization and/or cooperation between them. Besides, note that our study is topology-agnostic. The only assumption we make is that a secondary system transmits on spectral resources adjacent to a CP-OFDM based incumbent, and we then explore the consequences of the secondary utilizing a FB-MC waveform on the coexistence capabilities of the considered users.

Note that such a coexistence scenario can occur in multiple use cases. A non-comprehensive list of examples is represented in Fig. 2. For instance, Fig 2a encompasses a situation in which a cellular LTE network is deployed and one of the free resource blocks (RBs) of its uplink band is reused by an autonomous D2D link between two devices. This kind of policy is of prime interest as it enables the network to use resources which would otherwise be left vacant. However, in that particular case, the D2D link could cause harmful interference to the LTE base station. Such scenarios have been investigated in [29], [33], and [34]. In Fig 2b, a situation in which some wireless local area networks (WLAN) are deployed in TV white spaces (TVWS) is represented. In that case, WLAN users could harm TV reception of primary users. This type of coexistence scenario has been widely investigated since the FCC took the decision to allow secondary communications to take place in TV white spaces [19], [26], [35]. In Fig. 2c, we give a

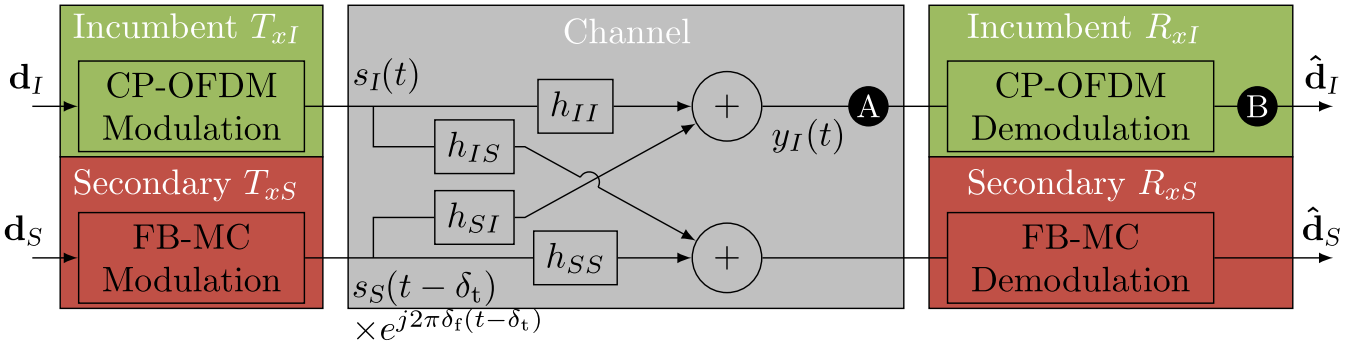

FIGURE 4. System model used to tackle the coexistence between the incumbent and secondary systems. White Gaussian noise is neglected to keep the focus on inter-system interference caused by the coexistence between the two systems. Timing and frequency misalignment factors are introduced to reflect the fact that there is no inter-system synchronization. We represent points A and B for future reference.

last example of a mesh ad-hoc network utilizing the 2.4 GHz industrial, scientific and medical (ISM) band, thus causing harmful interference to a neighboring Wi-Fi access point. In all of these examples, application and network topology vary, but one thing remains: a secondary system coexists with a CP-OFDM based incumbent one on the same frequency band.

B. LIMITATION OF CURRENT COEXISTENCE STUDIES

In this article, we do not claim to address a new problem: a number of studies analyzing coexistence between various waveforms in heterogeneous scenarios have been led in the literature [7], [19]–[21], [28]. Rather, we claim that the way these analysis have been led so far is insufficient, and propose an alternative approach. Indeed, most available studies only rely on the observation of the spectrum to rate the coexistence capabilities of various systems.

Based on the observation of the spectrum only, most studies directly conclude that waveforms with improved spectral localization are best suited to coexist with CP-OFDM based incumbent systems. These works rely on the PSD-based model that we will introduce in Section IV. However, with this approach, the gains are difficult to quantize precisely, and more accurate models are needed. In the following, we therefore introduce a simple model that we will use in the following of this article to study the coexistence between one FB-MC secondary and one incumbent CP-OFDM system.

C. SYSTEM MODEL

Let us lay out a simple system model consisting of a secondary system, S, and an incumbent system I, that coexist in a spectral band and both use a certain set of subcarriers, respectively $\mathcal{M}_S$ and $\mathcal{M}_I$, as is shown in Fig. 3. The incumbent system I is composed of a pair of CP-OFDM users, whereas the users forming the secondary system S are based on an alternative FB-MC waveform, as depicted in Fig. 4. We show that in each system, the vector $\mathbf{d}$ containing the symbols to be transmitted is fed to the waveform modulator. Then the signals transmitted by both systems are added in the wireless channel and received by both systems which demodulate the received signal and detect the vector of estimated symbols $\hat{\mathbf{d}}$.

Therefore, each system may interfere on the other in function of the properties of the transmitted signals and the demodulation operations that are performed at the receive end.

Two main specificities of the system model presented in Fig. 4 must be pointed out. In the first place, we do not take into account addtitive white Gaussian noise (AWGN). This is done deliberately to put the focus of this work on inter-system interference. Besides, as previously mentioned in introduction, a core part of our analysis lies in the fact that the secondary and the incumbent users coexist without pursuing any collaboration and/or synchronization between them. Therefore, it is most likely that both systems will disagree on the time and frequency basis.

To encompass this effect, we introduce two parameters:

1) **Time misalignment** δ_t: as the incumbent and secondary systems do not synchronize their transmission in time, we assume that the secondary system starts its transmission with a certain random delay δ_t with respect to the incumbent system.
2) **Frequency misalignment** δ_f: local oscillators (LOs) of mobile terminals have a typical accuracy of ± 1 ppm with respect to their nominal frequency [36]. For example, at a carrier frequency of 2 GHz, this can yield a misalignment between users of around 10^4 Hz, which can become significant as it is close to the LTE subcarrier width of 15 kHz. Therefore, as the incumbent and secondary systems do not cooperate, we assume that the secondary system misaligns its carrier frequency of a factor δ_f with respect to the incumbent system. However, note that we consider that the transmitter and receiver in each separate system achieve perfect frequency synchronization.

Taking into account these two factors, the signal received at the input antenna of the incumbent CP-OFDM receiver is, as shown in Fig. 4,

$$y_I(t) = h_{II}(t) \star s_I(t) + h_{SI}(t) \star s_S(t-\delta_t) e^{j2\pi\delta_f(t-\delta_t)}, \quad (1)$$

in which h_{II} is the channel between the incumbent transmitter and the incumbent receiver, whereas h_{SI} is the channel between the secondary transmitter and the incumbent receiver. In our work, we will first consider flat channels and only take into account pathloss effects to keep the focus on the interference created by the reception of a FB-MC signal by a CP-OFDM receiver. Nevertheless, we will in a second step extend our study to multipath channels to take frequency fading into account in Section VI. In order to build up on this system model, we present in the following section the signal models of the CP-OFDM and FB-MC waveforms that the incumbent and secondary systems can use.

III. WAVEFORMS BACKGROUND AND SIGNAL MODELS

A. GENERIC MULTICARRIER WAVEFORM MODEL

We consider a multi-carrier system with M subcarriers, time spacing between symbols ΔT and subcarrier spacing ΔF. Then, the time-domain continuous baseband signal that is transmitted by this system is written as

$$s(t) = \sqrt{P}\sum_{m=0}^{M-1}\underbrace{\sum_{n\in\mathbb{Z}}\mathbf{d}_m[n]f_{n,\mathrm{T}}(t-n\Delta\mathrm{T})e^{j2\pi m\Delta\mathrm{F}(t-n\Delta\mathrm{T})}}_{s_m(t)}, \quad \forall t\in\mathbb{R}, \quad (2)$$

where P is the transmit power, $\mathbf{d}_m$ is the vector of unitary power symbols that are transmitted on the mth subcarrier, and $f_{n,\mathrm{T}}$ is the transmit filter used to transmit the nth symbol on each subcarrier by the multi-carrier system.

In our work, we assume perfect synchronization in both time and frequency between the transmitter and the receiver of the same system. Under this assumption, on a flat channel, the received signal $y(t)$ is expressed as

$$y(t) = \sqrt{G}s(t), \quad (3)$$

where G is the channel gain. The obtained signal y is then demodulated and the vector of estimated symbols on each subcarrier is expressed as

$$\hat{\mathbf{d}}_m[n] = \int_{-\infty}^{+\infty} f_{n,\mathrm{R}}(t-n\Delta\mathrm{T})e^{-j2\pi m\Delta\mathrm{F}(t-n\Delta\mathrm{T})}y(t)\mathrm{d}t, \quad (4)$$

where $f_{n,\mathrm{R}}$ is the receive filter used on each subcarrier to demodulate the nth incoming symbol. Based on this generic model, we can describe any waveform, either CP-OFDM or FB-MC, by simply defining the parameters $f_{n,\mathrm{T}}$, $f_{n,\mathrm{R}}$, ΔT and ΔF. In the following, we configure this generic model for the waveforms of interest to this study.

B. CP-OFDM

In our framework, CP-OFDM systems are classically defined by the following set of parameters:

- $\Delta\mathrm{T} = T + T_{\mathrm{CP}}$
- $\Delta\mathrm{F} = \frac{1}{T}$
- $\forall n\in\mathbb{Z}, f_{n,\mathrm{T}}(t) = f_{\mathrm{T}}(t) = \begin{cases}\frac{1}{\sqrt{T}}, & t\in[-T_{\mathrm{CP}}, T]\\ 0, & \text{elsewhere}\end{cases}$
- $\forall n\in\mathbb{Z}, f_{n,\mathrm{R}}(t) = f_{\mathrm{R}}(t) = \begin{cases}\frac{1}{\sqrt{T}}, & t\in[0, T]\\ 0, & \text{elsewhere}\end{cases}$

C. LINEAR CONVOLUTION-BASED FILTER BANKS

The main difference between CP-OFDM and linear FB-MC systems lies in the fact that the latter use a selective prototype filter g of length T_g on each subcarrier to improve their spectral localization compared to CP-OFDM. Note that these systems usually use real symmetric filters so that $g^*(-t) = g(t)\forall t\in\mathbb{R}$. Therefore, every linear convolution based FB-MC system has the following set of transceive filter:

- $\forall n\in\mathbb{Z}, f_{n,\mathrm{T}}(t) = f_{\mathrm{T}}(t) = \begin{cases}g(t), & t\in\left[-\frac{T_g}{2}, \frac{T_g}{2}\right]\\ 0, & \text{elsewhere}\end{cases}$
- $\forall n\in\mathbb{Z}, f_{n,\mathrm{R}}(t) = f_{\mathrm{R}}(t) = \begin{cases}g(t), & t\in\left[-\frac{T_g}{2}, \frac{T_g}{2}\right]\\ 0, & \text{elsewhere}\end{cases}$

Based on this structure, linear FB-MC waveforms can come in different flavours according to the values taken by the input symbols $\mathbf{d}_m[n]$ and the parameters ΔT and ΔF. We specify this in the following.

1) FMT [11], [12]

In FMT, the harmful inter-carrier interference introduced by prototype filter g is countered by introducing a guard band of width W_{GB} between every subcarrier, which comes at the cost of spectral efficiency. Therefore, FMT systems use the following set of parameters: $\Delta\mathrm{T} = T$, $\Delta\mathrm{F} = \frac{1}{T} + W_{\mathrm{GB}}$

2) OFDM/OQAM [13], [14]

To achieve both optimal spectral efficiency and good spectral localization, OFDM/OQAM systems transmit real symbols drawn from a pulse amplitude modulation (PAM). A $\frac{\pi}{2}$ phase difference is then added between subsequent symbols and they are transmitted at twice the symbol rate $\frac{2}{T}$. As a result of this, orthogonality in the real domain is achieved. Therefore, OFDM/OQAM is based on the following set of parameters: $\Delta\mathrm{T} = \frac{T}{2}$, $\Delta\mathrm{F} = \frac{1}{T}$

3) FBMC-PAM [15]

One of the problems of OFDM/OQAM lies in the doubling of the symbol rate. A recent alternative, called FBMC-PAM or Lapped FBMC consists in doubling the number of subcarriers and multiplying each symbol by a certain phase factor $\phi_{m,n} = (n - \frac{1}{2} + \frac{M}{2})(m - \frac{1}{2})$. As a result, this modulation also achieves real orthogonality and has the following parameters: $\Delta\mathrm{T} = T$, $\Delta\mathrm{F} = \frac{1}{2T}$

D. CIRCULAR CONVOLUTION-BASED FILTER BANKS

To avoid the detrimental delay incurred by linear convolution, circular convolution based filter banks are based on convolution with circularly shifted versions of the prototype filter g. Based on this idea, two main waveforms have been

proposed.

1) GFDM [16], [17]

In GFDM, complex symbols are modulated per block of N_b and a CP of length T_CP is added between every subsequent block. Therefore, from an initial prototype filter g, GFDM systems define a set of N_b filters defined as, $\forall n \in [0, N_\mathrm{b}-1]$,

$$\tilde{g}_n(t) = \begin{cases} g(t - nT \bmod N_\mathrm{b}T), & t \in [-T_\mathrm{CP}, N_\mathrm{b}T] \\ 0 & \text{elsewhere.} \end{cases} \quad (5)$$

Therefore, GFDM systems utilize the following set of transceive filters and parameters:

- $\forall n \in \mathbb{Z}, f_{n,\mathrm{T}}(t) = \begin{cases} \tilde{g}_{n \bmod N_\mathrm{b}}(t), & t \in [-T_\mathrm{CP}, N_\mathrm{b}T] \\ 0, & \text{elsewhere} \end{cases}$
- $\forall n \in \mathbb{Z}, f_{n,\mathrm{R}}(t) = f_\mathrm{R}(t) = \begin{cases} \tilde{g}_{n \bmod N_\mathrm{b}}, & t \in [-T_\mathrm{CP}, N_\mathrm{b}T] \\ 0, & \text{elsewhere} \end{cases}$
- $\Delta\mathrm{T} = N_\mathrm{b}T + T_\mathrm{CP}, \ \Delta\mathrm{F} = \frac{1}{T}$

2) COQAM [18]

GFDM suffers from the same limitations imposed by the BLT as linear convolution based FB-MC. Therefore, GFDM based systems need to compensate for inter-carrier interference through specific receiver schemes. Another possibility is to adapt the OQAM modulation to GFDM, a proposal called COQAM. This system is essentially similar to GFDM, the only difference lying in the fact that, as it is based on OQAM, real symbols are transmitted at half the symbol rate. Therefore, according to our model, $2N_\mathrm{b}$ prototype filters are defined from the original prototype filter g as $\forall n \in [0, 2N_\mathrm{b}-1]$,

$$\tilde{g}_n(t) = \begin{cases} g(t - n\frac{T}{2} \bmod N_\mathrm{b}T), & t \in [-T_\mathrm{CP}, N_\mathrm{b}T] \\ 0 & \text{elsewhere.} \end{cases} \quad (6)$$

The rest of the parameters are defined exactly as for GFDM.

Note that, because of the circular convolution, GFDM and COQAM have poorer spectral containment than linear convolution based FB-MC waveforms. To solve this problem, a number of research works have proposed to add windowing and/or filtering on top of GFDM or COQAM modulations [17], [18]. We deliberately ignore these solutions in our analysis, as we are interested in studying how the intrinsic filtering properties of the presented waveforms may improve coexistence with CP-OFDM based users.

E. SUMMARY AND PSD COMPARISON

Based on the above presentation of CP-OFDM and FB-MC waveforms, we summarize in Table 1 the set of parameters and prototype filters used by each waveform. The values set in this table will be used in the remaining of this study. In order to have a fair point of comparison, we fix $\Delta\mathrm{F} = 1$ for reference for each waveform, with the exception of FBMC-PAM which uses subcarriers that are only half as wide as those of other systems.

TABLE 1. Parameters used by described waveforms.

	CP-OFDM	FMT	OFDM/OQAM	FBMC-PAM	GFDM	COQAM
$\Delta\mathrm{F}$	1			$\frac{1}{2}$	1	
T	$\frac{1}{\Delta\mathrm{F}}$	$\frac{1}{\Delta\mathrm{F}-W_\mathrm{GB}}$	$\frac{1}{\Delta\mathrm{F}}$			
$\Delta\mathrm{T}$	$T+T_\mathrm{CP}$	T	$\frac{T}{2}$	T	$N_\mathrm{b}T+T_\mathrm{CP}$	
g		RRC, roll-off 1	Phydyas [37]	Sine filter [15]	RRC, roll-off 1	
T_g		$6T$	$4T$	$2T$	$5T$	
N_b					5	
T_CP	$\frac{T}{8}$				$\frac{T}{8}$	
W_GB		$\frac{\Delta\mathrm{F}}{9}$				

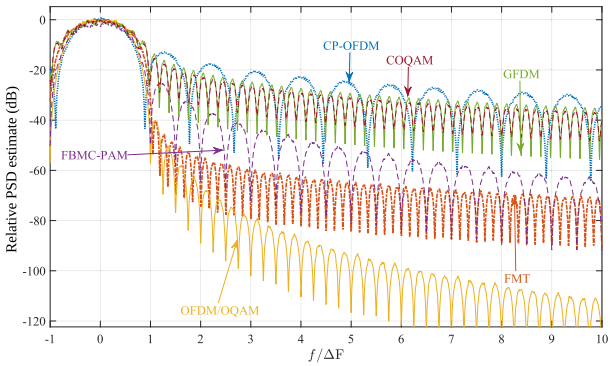

FIGURE 5. Welch estimate of the PSD level of studied waveforms with a Hanning Window of length $\frac{100}{\Delta\mathrm{F}}$ and a frequential resolution of 500 points per subcarrier. PSD values are expressed relatively to their maximum.

In Fig. 5, we present the PSD of one subcarrier of the aforementioned waveforms with the chosen parameters. Note that, to achieve a fair comparison, we considered that not one, but two adjacent subcarriers of the FBMC-PAM system were active. Moreover, it is important to recall that the presented PSD curves correspond to theoretical values that do not take into account hardware impairments and nonlinearities. In real systems, the sidelobes of each waveform would be increased [38]. It appears clearly that circular convolution based FB-MC systems do not achieve satisfying spectral containment, opposed to linear convolution based FB-MC systems whose sidelobes decrease much more rapidly. Following the idea presented in Section II-B, it is expected that the waveforms with better spectral containment will be better suited for coexistence with CP-OFDM based legacy systems. In the literature, this has usually been quantified through the use of the PSD-based model, which we present in the following.

IV. PSD-BASED MODELING OF INTERFERENCE

A. MODEL DEFINITION

The PSD-based model consists in computing the leakage caused by users onto each other by integrating the PSD of the interfering signal on the band that suffers from the interference. In the scenario we consider, defining $I_\mathrm{PSD}^{\mathrm{S}\to\mathrm{I}}$ the interference injected by the secondary system onto the

incumbent one according to the PSD based model, it is expressed as

$$I_{\text{PSD}}^{\text{S}\to\text{I}} = P_{\text{S}} G_{SI} \int_{\mathcal{M}_{\text{I}}} \Phi_{\text{S}}(f) df, \tag{7}$$

where Φ_{S} represents the PSD of the secondary signal modulated by secondary system S, P_{S} is the transmit power of the secondary and G_{SI} is the gain associated with the channel h_{SI}.

Considering that the secondary system modulates i.i.d. symbols with unitary power on each subcarrier, its PSD is defined as

$$\forall f \in \mathbb{R}, \Phi_{\text{S}}(f) = \sum_{m\in\mathcal{M}_{\text{S}}} \Phi_m(f) = \sum_{m\in\mathcal{M}_{\text{S}}} \Phi_{\text{WF,S}}(f - m\Delta\text{F}), \tag{8}$$

where $\Phi_{m,\text{S}}(f)$ is the PSD of the mth subcarrier of system S, and is directly obtained from $\Phi_{\text{WF,S}}$, the PSD of one subcarrier of the waveform used by the secondary system, as presented in Fig. 5. Therefore, it follows that, according to the PSD-based model,

$$I_{\text{PSD}}^{\text{S}\to\text{I}} = \sum_{m_s\in\mathcal{M}_{\text{S}}} \sum_{m_i\in\mathcal{M}_{\text{I}}} I_{\text{PSD}}^{\text{S}\to\text{I}}(m_s - m_i), \tag{9}$$

with

$$\forall l \in \mathbb{Z}, I_{\text{PSD}}^{\text{S}\to\text{I}}(l) = P_{\text{S}} G_{SI} \int_{l\Delta\text{F}-\frac{\Delta\text{F}}{2}+\delta\text{f}}^{l\Delta\text{F}+\frac{\Delta\text{F}}{2}+\delta\text{f}} \Phi_{\text{WF,S}}(f) df. \tag{10}$$

With this notation, $I_{\text{PSD}}^{\text{S}\to\text{I}}(l)$ corresponds to the amount of interference injected by a certain subcarrier m_s of the secondary onto a subcarrier m_i of the incumbent such that $m_s - m_i = l$.

B. RESULTS OBTAINED BY EACH WAVEFORM

Having defined the PSD-based model, we present in Table 2 the values of $I_{\text{PSD}}^{\text{S}\to\text{I}}(l)$ obtained for all studied waveforms in the case where $P_{\text{S}} G_{SI} = 0\ dB$ and $\delta\text{f} = 0$. As expected, we see that the PSD-based model predicts that waveforms with better spectral localization will inject the lowest amount of interference onto the incumbent CP-OFDM system.

In details, we see clearly that the PSD-based model predicts that OFDM/OQAM, FMT and FBMC-PAM can be used efficiently to coexist with CP-OFDM incumbent systems. On the contrary, GFDM and COQAM systems only reduce the interference onto incumbent systems by 5 dB compared to CP-OFDM based secondary systems. This is caused by the circular filtering which incurs steep variations in the transmit signal and therefore causes projections on the whole spectrum.

C. LIMITATIONS OF THE PSD-BASED MODEL

Though the PSD-based model presented above is widely used in the literature, it suffers some limitations: for example, being based purely on frequency considerations, it is unable to encompass phenomenons related to time synchronism. This was already tackled by Medjahdi *et. al.* in [27]. However, the analysis carried out in that article was focused on homogeneous scenarios, in which the coexisting systems were both using the same waveform, either OFDM/OQAM or CP-OFDM. In that scenario, results showed that the main drawback of the PSD-based model lies in the fact that it cannot encompass time asynchronism between coexisting systems. This is a major drawback that does not enable us to analyze the effects of the time misalignment δ_{t} that we introduced in our system model in Section II-C.

TABLE 2. Interference tables in dB computed according to the PSD-based model for studied waveforms.

l	CP-OFDM	FMT	OFDM/OQAM	FBMC-PAM	GFDM	COQAM
0	-1.28	-1.26	-0.99	-2.64	-1.59	-1.47
1	-12.3	-10.8	-12.3	-13.1	-10.0	-10.3
2	-20.1	-57.2	-65.4	-37.2	-24.1	-24.7
3	-23.9	-62.7	-80.7	-45.3	-28.1	-28.9
4	-26.4	-65.7	-89.6	-50.6	-30.8	-31.5
5	-28.0	-68.0	-96.1	-54.6	-32.8	-33.4
6	-29.2	-70.0	-101.	-58.0	-34.2	-35.0
7	-30.3	-71.0	-105.	-60.6	-35.5	-36.2
8	-31.4	-72.2	-109.	-63.0	-36.7	-37.4
9	-32.6	-73.2	-112.	-65.1	-37.8	-38.5

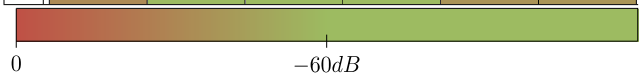

Moreover, it is clear that the interference computed by the PSD-based model I_{PSD} is measured **in the wireless channel**. This means that only the spectral properties of the interfering signal are taken into account. In other words, the PSD-based model computes the interference **at the input antenna** of the victim receiver, a point marked as Ⓐ in the system model scheme presented in Fig. 4. However, the values of interference that really matter are those experienced by the victim receiver after it demodulates the incoming signal, just before the decision, in other words at point Ⓑ in Fig. 4. Nevertheless, in the literature, the PSD-based model has been used to evaluate the ability of FB-MC based systems to coexist with other systems potentially based on CP-OFDM, for example to estimate the size of the guard band that would be necessary for the two systems to coexist [7], [19]–[21]. However, these conclusions should instead be based on measurements of the error vector magnitude (EVM) at the incumbent receiver that suffers from the adjacent transmission of the secondary system. This approach is indeed necessary to encompass both the properties of the transmitted secondary signal and the demodulation operations performed by the incumbent receiver. In fact, the PSD-based model only accounts for the properties of the transmitted secondary signal and omits the operations performed by the incumbent receiver. An illustration of how the PSD-based and EVM-based measurement of interference differ in their approach is given in Fig. 6.

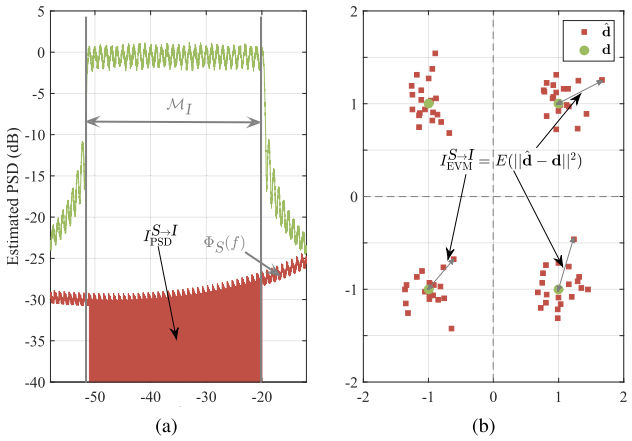

FIGURE 6. Comparison between (a) the PSD-based modeling of interference and (b) the EVM-based measure. Note that this representation is given in the case where the two signals arrive with the same power at the receiver, i.e., $P_S G_{SI} = P_I G_{II}$. The PSD-based modeling of interference consists in integrating the PSD of the interfering signal on the band of interest, and therefore does not take into account the receive operations performed at the victim receiver. Interference should rather be measured through EVM at the level of the decoded constellation, just before the symbol decision, as shown on (b).

It is clear that the EVM-based approach is much more representative of the actual interference experienced by the incumbent receiver. Namely, Medjahdi *et. al.* followed a similar approach under a different name in [27] to overcome the limitations of the PSD-based model in their specific scenario where the secondary and incumbent systems use the same waveform. However, in the heterogeneous scenario we study here, getting closed forms of the EVM may be challenging, as it involves much more intricate mathematical derivations than simply integrating the PSD. Therefore, it would be tempting to stick to the PSD based approach in the hope that values given by this model are close enough to the actual EVM values. This is what we propose to (in)validate in the following section by comparing values of interference obtained with the PSD-based model to values obtained through numerical simulations of the EVM.

V. EVM-BASED MEASUREMENT OF INTERFERENCE

A. PRINCIPLE OF THE EVM-BASED MEASURE OF INTERFERENCE

Consider the system model depicted in Fig. 4. In the following, parameters indexed as $\cdot_{\text{I}}$ and $\cdot_{\text{S}}$ refer to the incumbent and secondary system respectively. According to (4) and the expression of the CP-OFDM receive filter given in Section III-B, at point Ⓑ of Fig. 4, the demodulated symbol on the n_{I}th time slot and m_{I}th subcarrier of the incumbent is expressed as

$$\hat{\mathbf{d}}_{m_{\text{I}}}[n_{\text{I}}] = \frac{1}{\sqrt{T_{\text{I}}}} \int_{n_{\text{I}}(T_{\text{I}}+T_{\text{CP,I}})}^{n_{\text{I}}(T_{\text{I}}+T_{\text{CP,I}})+T_{\text{I}}} e^{-j2\pi \frac{m_{\text{I}}}{T_{\text{I}}}(t-n_{\text{I}}(T_{\text{I}}+T_{\text{CP,I}}))} y(t)\mathrm{d}t. \tag{11}$$

Recalling the expression of $y(t)$ given in (1), after some trivial derivations, we obtain

$$\hat{\mathbf{d}}_{m_{\text{I}}}[n_{\text{I}}] = \sqrt{P_I G_{II}}\mathbf{d}_{m_{\text{I}}}[n_{\text{I}}] + \boldsymbol{\eta}_{m_{\text{I}}}[n_{\text{I}}], \tag{12}$$

where $\boldsymbol{\eta}_{m_{\text{I}}}[n_{\text{I}}]$ represent the interference caused by the secondary FB-MC signal and is expressed as

$$\boldsymbol{\eta}_{m_{\text{I}}}[n_{\text{I}}] = \sqrt{\frac{P_S G_{SI}}{T_{\text{I}}}} \int_{n_{\text{I}}(T_{\text{I}}+T_{\text{CP,I}})}^{n_{\text{I}}(T_{\text{I}}+T_{\text{CP,I}})+T_{\text{I}}} e^{-j2\pi \frac{m_{\text{I}}}{T_{\text{I}}}(t-n_{\text{I}}(T_{\text{I}}+T_{\text{CP,I}}))} \times s_{\text{S}}(t-\delta_{\text{t}}) e^{j2\pi\delta_{\text{f}}(t-\delta_{\text{t}})}\mathrm{d}t. \tag{13}$$

Then, inserting (2) in (13), and operating the change of variable $t \mapsto t - n_{\text{I}}(T_{\text{I}} + T_{\text{CP,I}})$, we obtain

$$\boldsymbol{\eta}_{m_{\text{I}}}[n_{\text{I}}] = \sum_{m_{\text{S}}\in\mathcal{M}_{\text{S}}} \sum_{n_{\text{S}}\in\mathbb{Z}} \mathbf{d}_{m_{\text{S}}}[n_{\text{S}}] \sqrt{\frac{P_S G_{SI}}{T_{\text{I}}}} \times \int_0^{T_{\text{I}}} \left[f_{n_{\text{S}},\text{T}}(t-\tau(n_{\text{S}},n_{\text{I}})) e^{j2\pi[\nu(m_{\text{S}},m_{\text{I}},\delta\text{f})t+\phi(m_{\text{S}},m_{\text{I}},\delta\text{f},\delta\text{t})]} \right] \mathrm{d}t, \tag{14}$$

with

$$\tau(n_{\text{S}}, n_{\text{I}}) = n_{\text{S}}\Delta\text{T}_{\text{S}} - n_{\text{I}}\Delta\text{T}_{\text{I}} + \delta\text{t} \tag{15}$$

$$\phi(m_{\text{S}}, m_{\text{I}}, \delta\text{f}, \delta\text{t}) = -(m_{\text{S}}\Delta\text{F}_{\text{S}} + \delta\text{f})(n_{\text{S}}\Delta\text{T}_{\text{S}} - n_{\text{I}}\Delta\text{T}_{\text{I}}) - \delta\text{f}\delta\text{t} \tag{16}$$

$$\nu(m_{\text{S}}, m_{\text{I}}, \delta\text{f}) = m_{\text{S}}\Delta\text{F}_{\text{S}} - m_{\text{I}}\Delta\text{F}_{\text{I}} + \delta\text{f}. \tag{17}$$

Naming $C(m_{\text{S}}, m_{\text{I}}, n_{\text{S}}, n_{\text{I}}, \delta\text{f}, \delta\text{t})$ the integral term in (14), we have

$$\boldsymbol{\eta}_{m_{\text{I}}}[n_{\text{I}}] = \sum_{m_{\text{S}}\in\mathcal{M}_{\text{S}}} \underbrace{\sum_{n_{\text{S}}\in\mathbb{Z}} \mathbf{d}_{m_{\text{S}}}[n_{\text{S}}] \sqrt{\frac{P_S G_{SI}}{T_{\text{I}}}} C(m_{\text{S}}, m_{\text{I}}, n_{\text{S}}, n_{\text{I}}, \delta\text{f}, \delta\text{t})}_{\boldsymbol{\eta}_{m_{\text{S}}\to m_{\text{I}}}[n_{\text{I}}]}. \tag{18}$$

Then, the interference injected by the m_{S}th subcarrier of the secondary system onto the m_{I}th subcarrier of the incumbent system during the n_{I}th time-slot is expressed, according to our EVM approach, as

$$\mathbf{I}_{\text{EVM}}^{\text{S}\to\text{I}}(m_{\text{S}}, m_{\text{I}}, \delta\text{f}, \delta\text{t})[n_{\text{I}}] = E_{\mathbf{d}_{\text{S}}}\{|\boldsymbol{\eta}_{m_{\text{S}}\to m_{\text{I}}}[n_{\text{I}}]|^2\} \tag{19}$$

$$= \frac{P_S G_{SI}}{T_{\text{I}}} \sum_{n_{\text{S}}\in\mathbb{Z}} |C(m_{\text{S}}, m_{\text{I}}, n_{\text{S}}, n_{\text{I}}, \delta\text{f}, \delta\text{t})|^2. \tag{20}$$

Finally, in line with the approach in [27], we consider that δt is a random variable that is uniformly distributed in $[0, T_{\text{I}} + T_{\text{CP,I}}]$. This is done in order to encompass the lack of synchronization and coordination between the secondary and incumbent systems. Note that we keep a fixed value of δf as this parameter only shifts the secondary transmission in frequency. The final average value of measured interference is then obtained as the average EVM for all values of n_I and all possible realisations of δt as

$$I_{\text{EVM}}^{\text{S}\to\text{I}}(m_{\text{S}}, m_{\text{I}}, \delta\text{f}) = E_{\delta\text{t}}\left\{\overline{\mathbf{I}_{\text{EVM}}^{\text{S}\to\text{I}}(m_{\text{S}}, m_{\text{I}}, \delta\text{f}, \delta\text{t})}\right\}. \tag{21}$$

B. SIMULATION SETUP AND OBTAINED RESULTS

Though the EVM-based modeling of interference we presented is much more rigorous than the PSD-based approach, it is also much more convoluted and far less practical. In order to check if it is necessary to pursue the EVM-based modeling of interference, we simulate values obtained according to the model defined in (21). To do so, we consider the waveforms setups depicted in Table 1 and we set $\delta f = 0$. Thus, as in the PSD-based model, only the value of $m_S - m_I = l$ matters. For each waveform used by the secondary system, we measure the interference experienced on each subcarrier of the incumbent CP-OFDM system according to (21).

Obtained results are depicted in Fig. 7. Note that, in that figure, we plot both the results obtained with the EVM-based approach on the left side, and those obtained with the PSD-based model on the right side. Undeniably, the actual interference based on EVM measurements after the CP-OFDM demodulator is tremendously higher than what is predicted with the PSD-based model, at the input antenna of the incumbent receiver. The case of OFDM/OQAM based secondary systems gives a glaring example: at a subcarrier distance $l = 2$, the PSD-based model predicts that OFDM/OQAM will inject an interference power of -65.4 dB. In fact, simulated EVM values show that it is actually around -18.4 dB. This means that the PSD-based model underestimates more than 10 000 times some values of the interference experienced by the CP-OFDM incumbent system. Moreover, we see that the gains achieved by the secondary system if it uses FB-MC waveforms are dramatically reduced. Indeed, the interference caused onto the CP-OFDM incumbent receiver is only reduced by 1 to 3 dB if the secondary system uses a FB-MC waveform instead of CP-OFDM. Interestingly, the order of magnitude of this performance gap is quite in line with the results obtained by some of the experiments we cited in introduction, in particular [24], [25]. This brings two conclusions:

1) The PSD-based model evaluates the interference to CP-OFDM systems poorly and gives misleading results. Though it gives an approximation of interference in the channel, it cannot be used to predict the performance of the incumbent receiver. In particular, it does not give any valid insight on the advantages of FB-MC for coexistence with CP-OFDM.
2) Opposed to the common way of thinking, FB-MC waveforms do not drastically facilitate coexistence with incumbent CP-OFDM based legacy systems.

So, why is the PSD-based model so inaccurate? The main reason is given in Fig. 8: FB-MC systems rely on prototype filters that are longer than the time-symbol to achieve acute frequency localization. However, the CP-OFDM receiver filter is a rectangular window of length equal to the time-symbol. Therefore, it truncates the well-shaped prototype filter used to transmit the FB-MC secondary signal in parts that, on their own, are not particularly well frequency localized. As a result of this operation, the advantageous PSD

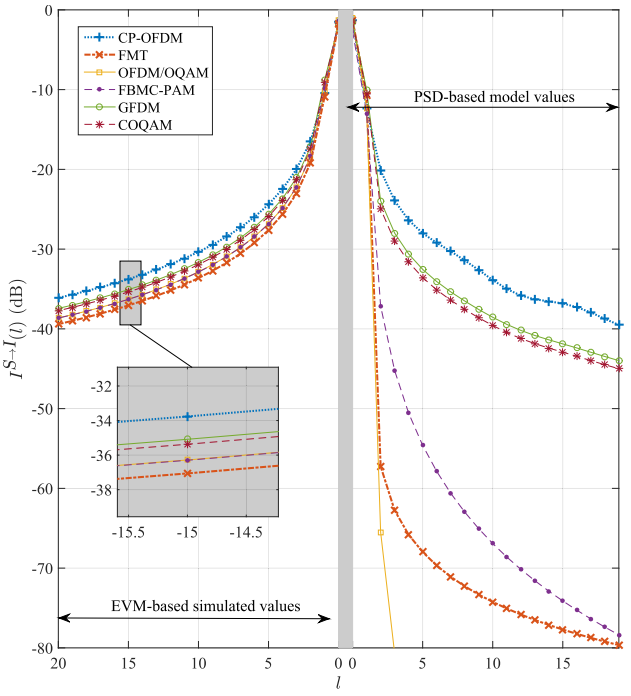

FIGURE 7. Interference caused onto a CP-OFDM based incumbent system by a secondary system based on multiple waveforms. Values predicted by the PSD-based model (right-hand side) are compared to those obtained through Monte-Carlo simulations of the average EVM at the incumbent CP-OFDM receiver according to (21) (left-hand side). Whatever the waveform used by the secondary system, EVM-based values are dramatically higher than those predicted by the PSD-based model. Results are shown for $P_S G_{SI} = 0dB$ and $\delta f = 0$. Note that any other value simply translates to a shift on the y-axis of all curves.

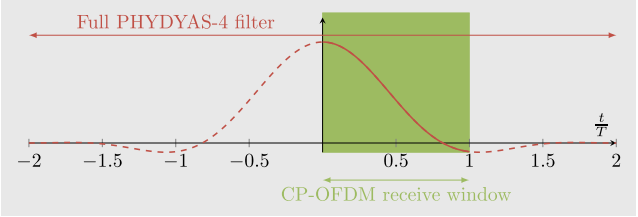

FIGURE 8. Key phenomenon that explains the difference between the EVM-based measurement of interference and the predictions of the PSD-based model: FB-MC waveforms use longer-than-T filters to achieve high spectral localization, but these are cut by the T-long receive window of the incumbent CP-OFDM system. Figure shows the example of an OFDM/OQAM based secondary with PHYDYAS-4 filter, but the same applies for any other FB-MC waveform. We point out that this effect arises even if there is no time or frequency misalignment between users, i.e., in cases where $\delta_t = \delta_f = 0$.

properties of the FB-MC signals are lost by the CP-OFDM incumbent receiver. Note that this is a general result that can be extended to virtually any signal passing through a CP-OFDM receiver. Indeed, the latter acts exactly as a poor spectrum analyzer which outputs high frequency ripples even when fed a well localized signal.

VI. ANALYTICAL ASPECTS

A. CLOSED FORMS DERIVATION

At this point of our discussion, the main ideas of this article have been exposed. To finish convincing the reader of the

$$|A_{\Pi_{T_\mathrm{I}},g}(\tau,\nu)| = \begin{cases} 0, & \tau > T_\mathrm{I} + \frac{T_g}{2} \text{ or } \tau < -\frac{T_g}{2}. \\ \left|(\tau + \frac{T_g}{2}) \sum_{k\in\mathbb{Z}} G_k e^{j\pi \frac{k}{T_g}(\frac{T_g}{2}-\tau)} \mathrm{sinc}(\pi(\frac{k}{T_g}+\nu)(\frac{T_g}{2}+\tau))\right|, & -\frac{T_g}{2} \le \tau \le T_\mathrm{I} - \frac{T_g}{2} \\ \left|(T_\mathrm{I} - (-\frac{T_g}{2}+\tau)) \sum_{k\in\mathbb{Z}} G_k e^{j\pi \frac{k}{T_g}(-\frac{T_g}{2}-\tau+T_\mathrm{I})} \mathrm{sinc}(\pi(\frac{k}{T_g}+\nu)(T_\mathrm{I} - (-\frac{T_g}{2}+\tau)))\right|, & \frac{T_g}{2} \le \tau \le T_\mathrm{I} + \frac{T_g}{2} \\ \left|T_\mathrm{I} \sum_{k\in\mathbb{Z}} G_k e^{j\pi \frac{k}{T_g}(T_\mathrm{I}-2\tau)} \mathrm{sinc}(\pi(\frac{k}{T_g}+\nu)T_\mathrm{I})\right|, & T_\mathrm{I} - \frac{T_g}{2} \le \tau \le \frac{T_g}{2} \end{cases} \quad (22)$$

validity of our claims, we derive in this section the mathematical analysis of the inter-system interference according to the mathematical model laid out in Section V-A. Let us fix m_I, m_S, δf and δt. In (20), $I^{\mathrm{S}\to\mathrm{I}}_{\mathrm{EVM}}(m_\mathrm{S}, m_\mathrm{I}, \delta\mathrm{f}, \delta\mathrm{t})$ is written as the sum of specific values of the magnitude of the cross-ambiguity function between the transmit filter of the secondary and a rectangular window.

In the case where the secondary system is based on linear convolution FB-MC, we reminded in Section III-C that the transmit filter used to modulate each subsequent symbol is equal to the used prototype filter g. Therefore, we can show that $|C(m_\mathrm{S}, m_\mathrm{I}, n_\mathrm{S}, n_\mathrm{I}, \delta\mathrm{f}, \delta\mathrm{t})|$ can be expressed as $\left|A_{\Pi_{T_\mathrm{I}},g}(\tau(n_\mathrm{S}, n_\mathrm{I}), \nu(m_\mathrm{S}, m_\mathrm{I}, \delta\mathrm{f}))\right|$, the cross-ambiguity function between a rectangular window of length T_I and the prototype filter g, with τ and ν following the expressions of (15), (17). The expression of $|A_{\Pi_T,g}|$ is given in (22), as shown at the top of this page, where the terms G_k represent the Fourier coefficients of the prototype filter g used by the secondary system. Developments leading to this expression are detailed in the Appendix. Therefore, (20) is rewritten as

$$\mathbf{I}^{\mathrm{S}\to\mathrm{I}}_{\mathrm{EVM}}(m_\mathrm{S}, m_\mathrm{I}, \delta\mathrm{f}, \delta\mathrm{t})[n_\mathrm{I}] = \frac{P_S G_{SI}}{T_\mathrm{I}} \times \sum_{n_\mathrm{S}\in\mathbb{Z}} |A_{\Pi_{T_\mathrm{I}},g}(\tau(n_\mathrm{S}, n_\mathrm{I}), \nu(m_\mathrm{S}, m_\mathrm{I}, \delta_\mathrm{f}))|^2. \quad (23)$$

Putting (22) in this last expression, we see clearly that the power of interference caused by the secondary FB-MC waveform onto the incumbent CP-OFDM system slowly decays in frequency, following a weighted sum of sinc functions. This last expression can be used to rate the exact interference seen on the n_Ith time slot of the incumbent system. This gives us a closed-form expression of the interference seen on each symbol of the incumbent CP-OFDM system, for a particular value of time misalignment δ_t between the two systems.

However, obtaining closed-form expressions of the average interference as expressed in (21) is impractical, because it involves taking the average value of the vector $\mathbf{I}^{\mathrm{S}\to\mathrm{I}}_{\mathrm{EVM}}(m_\mathrm{S}, m_\mathrm{I}, \delta\mathrm{f}, \delta\mathrm{t})$, and then take the expected value of the result with respect to random variable δ_t. Moreover, the results presented in Fig. 7 reduce the appeal for closed-form expressions. The main point we want to show in this analysis is that the CP-OFDM reception causes high interference to the incumbent system, which is explained by the appearance of the sinc function in (22).

Nevertheless, based on our previous works in [30] and [31], we can assert that the value of interference is in most cases only slightly dependent on the values of n_I and δt. Therefore, in order to offer tractable equations, it is possible to adopt the following approximation:

$$I^{\mathrm{S}\to\mathrm{I}}_{\mathrm{EVM}}(m_\mathrm{S}, m_\mathrm{I}, \delta\mathrm{f}) \approx \mathbf{I}^{\mathrm{S}\to\mathrm{I}}_{\mathrm{EVM}}(m_\mathrm{S}, m_\mathrm{I}, \delta\mathrm{f}, \delta\mathrm{t}=0)[0]. \quad (24)$$

With this approximated form, the expression of (21) simplifies into

$$I^{\mathrm{S}\to\mathrm{I}}_{\mathrm{EVM}}(m_\mathrm{S}, m_\mathrm{I}, \delta\mathrm{f}) \approx P_S G_{SI} T_\mathrm{I} \sum_{n=0}^{\frac{T_g}{\Delta T_\mathrm{S}}} \sum_{k\in\mathbb{Z}} G_k e^{j\pi \frac{k}{T_g}(T_\mathrm{I}-2(n\Delta T_\mathrm{S}))} \times \mathrm{sinc}(\pi(\frac{k}{T_\mathrm{g}}+\nu)T_\mathrm{I}). \quad (25)$$

Note that in the case where the secondary system uses circular convolution filter banks, the expression of (22) is not directly applicable. Indeed, because of the CP addition subsequent symbols pass through different filters that have slightly different Fourier coefficients. However, the main principle stays unchanged and (25) can be used as an approximation as well in the case of circular convolution FB-MC waveforms.

In Fig. 9, we compare the approximation of $I^{\mathrm{S}\to\mathrm{I}}_{\mathrm{EVM}}(m_\mathrm{S}, m_\mathrm{I}, \delta\mathrm{f})$ given in (25) with results obtained through Monte-Carlo simulations for $P_S G_{SI} = 1$. We see that the proposed approximation matches perfectly the simulated values for linear filter banks but only approximates the interference values in the case of circular filter banks, as predicted. Nevertheless, the obtained approximation is satisfying and shows well, for each waveform, that the interference to the CP-OFDM incumbent slowly decays, at approximately the same rate no matter what waveform is used by the secondary system. Note that we did not represent the curve for FBMC-PAM as it is clear from Fig. 7 that it interferes exactly as much as OFDM/OQAM.

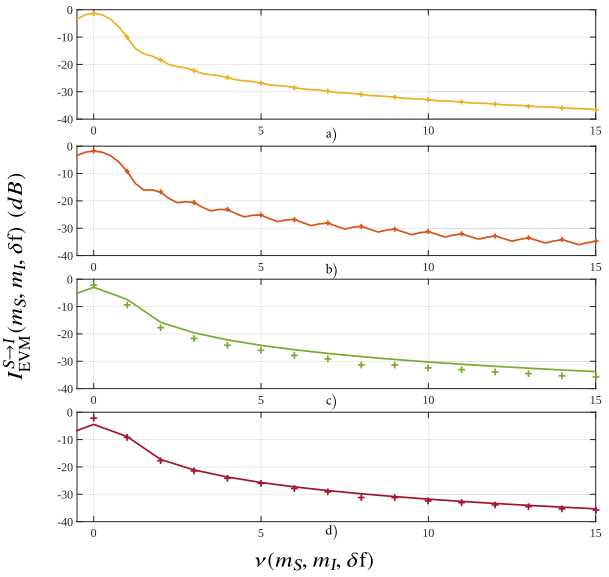

FIGURE 9. Comparison between simulated values of average interference based on EVM (crosses) and analytical approximation of (25) (solid line) for a) OFDM/OQAM, b) FMT, c) GFDM, and d) COQAM.

B. EXTENSION TO MULTIPATH CHANNELS

All throughout our study so far, we have considered flat channels which only affect the received power of the transmit signal and we have not taken into account the effects of noise. This enabled us to precisely evaluate the interference caused by any FB-MC signal on a CP-OFDM receiver. In this section, we detail how the model we developed can be applied to evaluate the performance of the incumbent CP-OFDM systems in realistic setups in which the multipath channel and Gaussian noise come into play. We recall that the multipath wireless channel can be modeled as a FIR filter as follows:

$$\forall t \in \mathbb{R},\ h(t) = \sqrt{G}\sum_{l=0}^{L-1} h_l \delta(t-\epsilon_l), \tag{26}$$

where L is the number of paths, h_l and τ_l are respectively the complex coefficient and delay associated with path l, and δ is the Dirac function. The coefficients h_l are defined as follows:

$$h_l \sim \mathcal{N}(0, \sigma_l^2) \tag{27}$$

$$\sum_l \sigma_l^2 = 1 \tag{28}$$

As is commonly known, if the CP used by the CP-OFDM transmission is longer than the maximum delay incurred by the channel, there is neither inter-symbol interference nor inter-carrier interference and the signal received by the incumbent can be directly obtained through channel equalization in the frequency domain.

1) ZERO FORCING (ZF) EQUALIZATION

If the incumbent system performs zero-forcing equalization, the symbols demodulated by the CP-OFDM incumbent receiver are obtained as follows:

$$\hat{\mathbf{d}}_{m_I}[n_I] = \frac{\sqrt{P_I G_{II}} H_{II,m_I} \mathbf{d}_{m_I}[n_I] + \mathbf{w}_{m_I}[n_I]}{\hat{H}_{II,m_I}} + \boldsymbol{\eta}_{m_I}[n_I], \tag{29}$$

where $\mathbf{w}_{m_I}[n_I]$ is the additional white Gaussian noise of variance σ_w^2. H_{II,m_I} is the channel response of channel h_{II} on the m_I-th subcarrier of the incumbent and $\hat{H}_{II,m_I}$ the estimate thereof. Classically, we can model the latter as

$$\hat{H}_{II,m_I} = H_{II,m_I} + \xi_{II,m_I}, \tag{30}$$

where $\xi_{II,m_I} \sim \mathcal{N}(0, \sigma^2_{\xi_{II,m_I}})$ represents the channel estimation error on subcarrier m_I. After trivial derivation steps, we obtain

$$\hat{\mathbf{d}}_{m_I}[n_I] = \sqrt{P_I G_{II}}\mathbf{d}_{m_I}[n_I] + \frac{\mathbf{w}_{m_I}[n_I]}{\hat{H}_{II,m_I}} + \boldsymbol{\rho}_{m_I}[n_I] + \boldsymbol{\eta}_{m_I}[n_I], \tag{31}$$

where $\boldsymbol{\rho}_{m_I}[n_I]$ is the part of error caused by imperfect channel estimation expressed as

$$\boldsymbol{\rho}_{m_I}[n_I] = -\frac{\xi_{II,m_I}\sqrt{P_I G_{II}}}{\hat{H}_{II,m_I}}\mathbf{d}_{m_I}[n_I]. \tag{32}$$

The effects of channel estimation errors are out of the scope of this study and we will therefore assume in the following that $\hat{H}_{II,m_I} = H_{II,m_I} \forall m_I$. The part of interference created by the secondary FB-MC signal that we are interested to model, $\boldsymbol{\eta}_{m_I}[n_I]$, is defined similarly as in (13) as

$$\boldsymbol{\eta}_{m_\mathrm{I}}[n_\mathrm{I}] = \frac{\sqrt{P_S}}{H_{II,m_I}\sqrt{T_\mathrm{I}}} \int_{n_\mathrm{I}(T_\mathrm{I}+T_{\mathrm{CP,I}})}^{n_\mathrm{I}(T_\mathrm{I}+T_{\mathrm{CP,I}})+T_\mathrm{I}} e^{-j2\pi\frac{m_\mathrm{I}}{T_\mathrm{I}}(t-n_\mathrm{I}(T_\mathrm{I}+T_{\mathrm{CP,I}}))} \times (h_{SI}(t) \star s_\mathrm{S}(t-\delta_\mathrm{t}))e^{j2\pi\delta_\mathrm{f}(t-\delta_\mathrm{t})}\mathrm{d}t. \tag{33}$$

With the definition of the multipath channel given in (26), we see that

$$h_{SS}(t) \star s_\mathrm{S}(t-\delta_\mathrm{t}) = \sqrt{G_{SI}}\sum_{l=0}^{L-1} h_{SI,l}\, s_\mathrm{S}(t-\delta_\mathrm{t}-\epsilon_{SI,l}). \tag{34}$$

Hence,

$$\boldsymbol{\eta}_{m_\mathrm{I}}[n_\mathrm{I}] = \frac{\sqrt{P_S G_{SI}}}{H_{II,m_I}\sqrt{T_\mathrm{I}}} \sum_{l=0}^{L-1} h_{SI,l} \int_{n_\mathrm{I}(T_\mathrm{I}+T_{\mathrm{CP,I}})}^{n_\mathrm{I}(T_\mathrm{I}+T_{\mathrm{CP,I}})+T_\mathrm{I}} e^{-j2\pi\frac{m_\mathrm{I}}{T_\mathrm{I}}(t-n_\mathrm{I}(T_\mathrm{I}+T_{\mathrm{CP,I}}))} \times s_\mathrm{S}(t-\delta_\mathrm{t}-\tau_{SI,l})e^{j2\pi\delta_\mathrm{f}(t-\delta_\mathrm{t}-\tau_{SI,l})}\mathrm{d}t. \tag{35}$$

This last equation is very interesting as we recognize a linear combination of the expression given in (13). Besides, if the channel h_{SI} can be assumed flat on each subcarrier, as is the

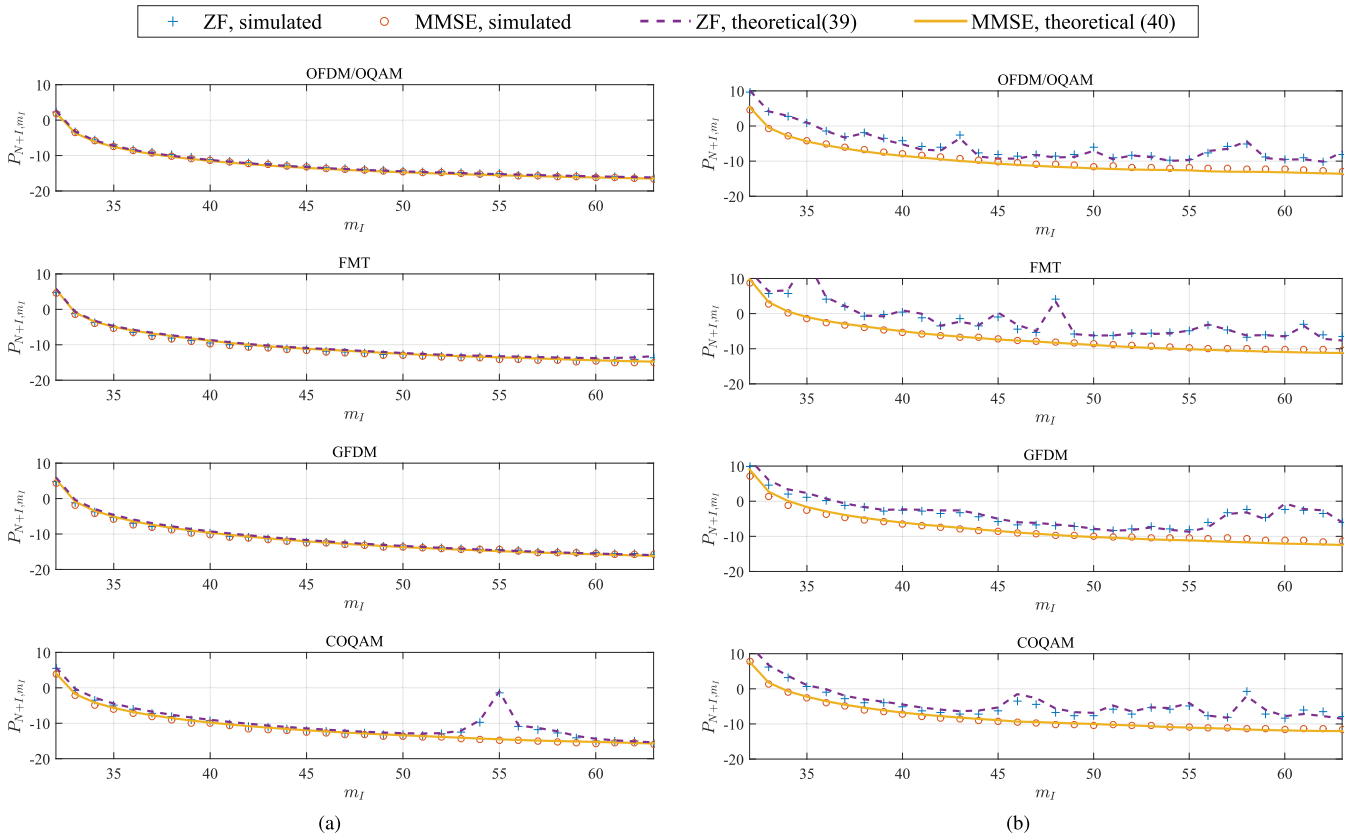

FIGURE 10. Average sum power of noise and interference in dB on each subcarrier m_I of the incumbent CP-OFDM system. Results are averaged over 1000 realizations of the secondary and incumbent channels, following the EPA (a) and ETU (b) channel models.

case in most communication scenarios, (35) can be simplified to

$$\begin{aligned}&\eta_{m_\mathrm{I}}[n_\mathrm{I}]\\&= \frac{\sqrt{P_S G_{SI}}}{H_{II,m_I}\sqrt{T_\mathrm{I}}} H_{SI,m_I} \int_{n_\mathrm{I}(T_\mathrm{I}+T_{\mathrm{CP,I}})}^{n_\mathrm{I}(T_\mathrm{I}+T_{\mathrm{CP,I}})+T_\mathrm{I}} e^{-j2\pi \frac{m_\mathrm{I}}{T_\mathrm{I}}(t-n_\mathrm{I}(T_\mathrm{I}+T_{\mathrm{CP,I}}))}\\&\quad\times s_\mathrm{S}(t-\delta_\mathrm{t}-\tau_{SI,l}) e^{j2\pi\delta_\mathrm{f}(t-\delta_\mathrm{t}-\tau_{SI,l})}\mathrm{d}t. \qquad (36)\end{aligned}$$

Then, following the exact same derivations as (14)-(25), we can conclude that

$$\begin{aligned}&I^{\mathrm{S}\to\mathrm{I}}_{\mathrm{EVM,ZF}}(m_\mathrm{S}, m_\mathrm{I}, \delta\mathrm{f})\\&\approx \frac{P_S G_{SI} T_\mathrm{I} |H_{SI,m_I}|^2}{|H_{II,m_I}|^2}\\&\quad\times \sum_{n=0}^{\frac{T_g}{\Delta T_\mathrm{S}}} \sum_{k\in\mathbb{Z}} G_k e^{j\pi\frac{k}{T_\mathrm{g}}(T_\mathrm{I}-2(n\Delta T_\mathrm{S}))} \mathrm{sinc}(\pi(\frac{k}{T_\mathrm{g}}+\nu)T_\mathrm{I}). \qquad (37)\end{aligned}$$

This last expression is very similar to (25) except for the factor $\frac{1}{|H_{II,m_I}|^2}$ which is due to the ZF equalization, and the factor $|H_{SI,m_I}|^2$ which represents the gain of the interfering channel on subcarrier m_I.

2) MINIMUM MEAN SQUARE ERROR (MMSE) EQUALIZATION

In the case of MMSE equalization, following the same derivations as in the ZF case, we obtain the following expression, analog to (37):

$$\begin{aligned}&I^{\mathrm{S}\to\mathrm{I}}_{\mathrm{EVM,MMSE}}(m_\mathrm{S}, m_\mathrm{I}, \delta\mathrm{f})\\&\approx \frac{P_S G_{SI} T_\mathrm{I} |H_{II,m_I} H_{SI,m_I}|^2}{\left||H_{II,m_I}|^2 + \frac{1}{\mathrm{SNR}_I}\right|^2}\\&\quad\times \sum_{n=0}^{\frac{T_g}{\Delta T_\mathrm{S}}} \sum_{k\in\mathbb{Z}} G_k e^{j\pi\frac{k}{T_\mathrm{g}}(T_\mathrm{I}-2(n\Delta T_\mathrm{S}))} \mathrm{sinc}(\pi(\frac{k}{T_\mathrm{g}}+\nu)T_\mathrm{I}), \qquad (38)\end{aligned}$$

where SNR_I is the SNR at the incumbent receiver. The derived expressions in the case of ZF and MMSE equalization show clearly that the model we developed on flat channel translates with very little modification to the multipath channel. In the following, we will demonstrate the validity of our model through simulations on multipath channels.

C. CASE STUDY

To demonstrate the validity of our approach, we consider a coexistence setup in which the secondary and the incumbent

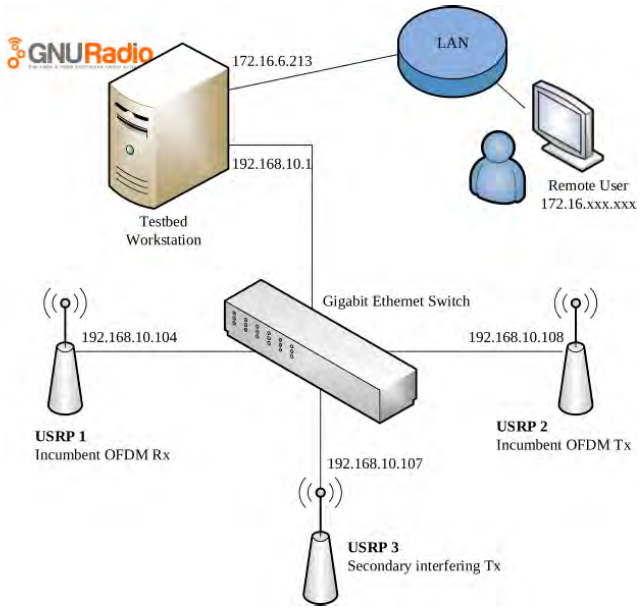

FIGURE 11. Experimentation setup: the three involved USRPs are in the same subnet and connected to the same gigabit ethernet switch as the testbed workstation. The latter acts as a gateway between the testbed subnet and the lab Local Area Network (LAN). Users can therefore access the workstation remotely and execute the GnuRadio application. Note that each USRP is also connected to an external clock source that is not represented in the figure.

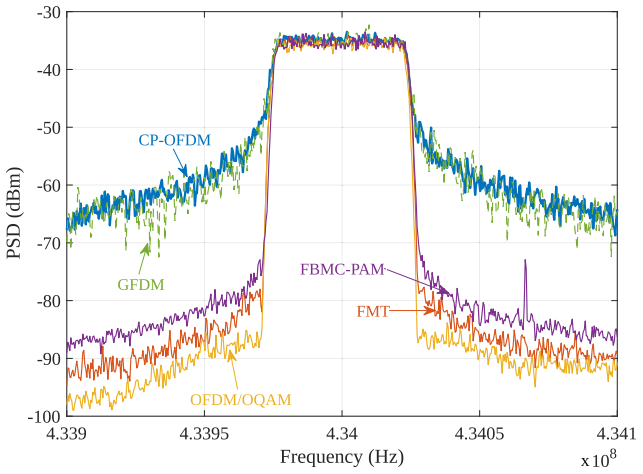

FIGURE 12. Comparison of the PSD of tested waveforms as seen on a spectrum analyzer. In our experiment, the high power amplifier functions almost perfectly linearly, and we are therefore able to reproduce experimentally the theoretical spectral shapes of FB-MC signals.

system are each allocated a band of 32 subcarriers. Furthermore, we consider that their active bands are directly adjacent such that $\mathcal{M}_S = \{0 \dots 31\}$ and $\mathcal{M}_I = \{32 \dots 63\}$. Moreover, we consider that the incumbent SNR, not accounting for the secondary interference, equals to $\frac{P_I G_{II}}{\sigma_w^2} = 20dB$. Besides, in order to put the focus on the effects of the interference caused by the secondary system, the secondary interfering transmitter is assumed to be closer to the incumbent receiver than the incumbent transmitter, so that $\frac{P_S G_{SI}}{P_I G_{II}} = 10\ dB$.

To verify the validity of our model in such a setup, we compute the average sum power of noise and interference on each subcarrier of the incumbent and compare it with the following predicted values in the case of ZF and MMSE equalization:

$$\text{ZF:} P_{N+I,m_I} = \frac{\sigma_w^2}{|H_{II,m_I}|^2} + \sum_{m_S \in \mathcal{M}_S} I^{\text{S}\to\text{I}}_{\text{EVM,ZF}}(m_\text{S}, m_\text{I}, \delta\text{f}). \tag{39}$$

$$\text{MMSE:} P_{N+I,m_I} = \frac{\sigma_w^2 |H_{II,m_I}|^2}{\left(|H_{II,m_I}|^2 + \sigma_w^2\right)^2} + \sum_{m_S \in \mathcal{M}_S} I^{\text{S}\to\text{I}}_{\text{EVM,ZF}}(m_\text{S}, m_\text{I}, \delta\text{f}). \tag{40}$$

In (39) and (40), the first term of the addition corresponds to the power of noise after equalization, which can be readily found in the literature, while the second term corresponds to the power of interference after equalization which we have characterized in (37) and (38) respectively. Results are shown on Fig. 10, in which we represent the simulated and predicted values of P_{N+I,m_I} on each subcarrier of the incumbent for both the ZF and MMSE equalizers. Note that the presented results have been averaged over 1000 realizations of the incumbent and secondary channel. These results show that the proposed model estimates the performance of the incumbent CP-OFDM system in a satisfying manner.

VII. EXPERIMENTAL VALIDATION

A. EXPERIMENTAL SETUP

To confirm and conclude our analysis, we developed a software radio testbed to analyze the coexistence scenario corresponding to Fig. 4 and validate the analytical expressions derived in the former section. The experiment consists of three Ettus USRP N210. Two USRPs are used to implement the incumbent OFDM transmission, and one USRP acts as the interfering secondary transmitter. Note that the secondary receiver is not included in this experiment as we focus on the interference caused by the secondary FB-MC system on the incumbent OFDM receiver.

The experiment is performed on the SCEE Testbed at CentraleSupélec. The two USRPs acting as the incumbent and secondary transmitters are both equipped with a SBX daughterboard and the incumbent receiver uses a WBX daughterboard. All USRPs are using a single VERT2450 antenna on their TX/RX RF frontend. To be able to control with ease the timing and frequency misalignements between all users, all USRPs are externally synchronized by an Ettus Research Octoclock-G which feeds each of them a reference 10 MHz clock and a pps signal. Moreover, all USRPs are connected to a gigabit ethernet switch and they are controlled by a workstation that is connected to the same switch. The experimentation software is written in python under the GnuRadio framework and executed on the workstation. The experiment is sketched in Fig. 11.

The communications take place in the 434 MHz ISM band. The OFDM incumbent system uses 256 subcarriers of width 1500 Hz, which corresponds to a total band of 384 kHz. The OFDM incumbent transmission is established on a subset

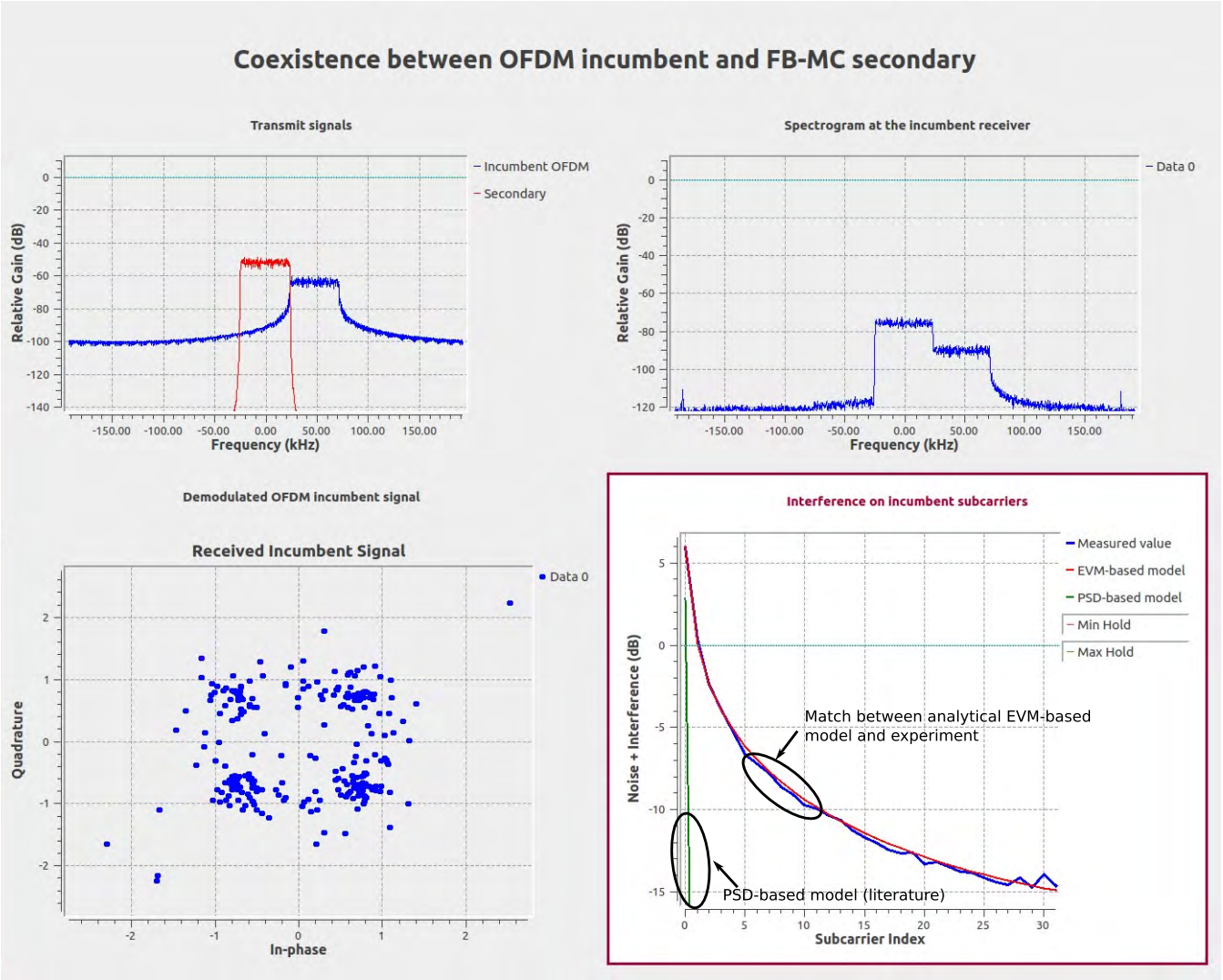

FIGURE 13. Developed GUI: the PSD of the FB-MC secondary signal (in red) and of the incumbent OFDM signal (in blue) are displayed on the top left quarter. The spectral shape of the signal received by the incumbent receiver is represented on the top right, and the constellation of the demodulated OFDM signal on the bottom left. The interference injected by the FB-MC transmitter on each subcarrier of the OFDM incumbent signal is plotted on the bottom right (blue curve) and compared to the literature PSD-based model (green curve) and our EVM-based model (red curve), which exhibits perfect accuracy.

of those 256 subcarriers, which is configurable at the initialization of the demonstration. On Fig. 13, we show an example in which the OFDM incumbent transmission happens on the subcarriers 16 to 47, and the secondary system transmits on a directly adjacent band, from subcarriers -16 to 15. The OFDM incumbent transmission is realized in real time through the use of custom GnuRadio OFDM blocks, while the secondary system is emulated by playing signals generated with Matlab. The secondary transmit signal can be set to one of the following waveforms: OFDM, FMT, OFDM/OQAM, FBMC-PAM, GFDM, COQAM. The transmit power of the secondary user can be dynamically varied at runtime.

It is well known that hardware impairments such as IQ imbalance or non-linearities of the high power amplifier can harmfully affect the theoretical spectral localization of the FB-MC waveforms we have shown in Fig. 5 [38]. However, these effects have been out of the scope of our study. Therefore, in our experimentation, we avoided these effects by precisely calibrating USRPs and ensuring that the high power amplifier was functioning in linear mode. To verify that we were able to transmit FB-MC waveforms with high spectral localization, we studied their spectral shape by plugging the output of the secondary USRP directly onto a spectrum analyzer. Results are represented in Fig. 12. We see clearly that, because the high power amplifier behaves linearly, the advantageous spectral shapes of the transmit FB-MC waveforms are preserved.

B. DEVELOPED GUI, OBTAINED RESULTS, AND DISCUSSION

To exploit the experimentation setup presented in Fig. 11, we developed a QT GUI on top of the GnuRadio application to dynamically manage the experiment and display results

in real time. The workflow of each experimentation can be described with the following steps:

1) The OFDM transmission is established, and sample synchronization is performed manually by finding the value for which no energy is leaked on inactive subcarriers.
2) Once sample synchronization is acquired, the OFDM receiver performs a very simple channel equalization: indeed, in the first step of the experiment, the OFDM transmitter is set to transmit only ones, so that the channel impulse response is equal to the received signal. The latter is simply inverted to perform ZF equalization of the channel.
3) Once sample synchronization and equalization have been performed, the OFDM transmitter starts emitting random 4-QAM symbols. The power of noise and interference on each subcarrier of the OFDM incumbent system is then plotted on the GUI, as is shown on Fig. 13.
4) We then start increasing the transmit power of the secondary interfering user so that the level of interference caused by the secondary system on the OFDM incumbent is much higher than the Gaussian noise. This allows us to compare the measured values of interference with both the PSD-based model from the literature and the EVM-based model we developed in the former section.

Note that the synchronization and equalization procedures performed by the OFDM incumbent system are deliberately kept simple. This is to keep the focus of our demonstration on the raw interference caused onto each subcarrier of the OFDM incumbent receiver. If we had set the OFDM transmission to use more advanced synchronization and equalization procedures based for example on pilot signaling, the interfering secondary signal may have altered the said pilot signals. As a result, the OFDM incumbent transmission may have been entirely lost and it would have been infeasible to compare the experimental results with our theoretical model.

On Fig. 13, we present the developed GUI in the state which is achieved after steps 1 to 4 explained above have been performed. Note that in that example, the secondary FB-MC system is using OFDM/OQAM. Moreover, as explained above, the secondary system is set to transmit at high power so that the effect of gaussian noise is negligible compared to the level of interference caused by the secondary system onto the incumbent. In turn, we see on the bottom right of Fig. 13 a near-perfect match between the value of interference measured on each OFDM incumbent subcarrier and the value predicted by the EVM-based model developed in Section VI. On the opposite, we see clearly that the PSD-based model fails to provide any valid estimation of the interference suffered by the incumbent. We observe similar results for FB-MC waveforms other than OFDM/OQAM.

VIII. CONCLUSION

In this paper, we investigated the coexistence on the same band of users utilizing FB-MC waveforms and legacy CP-OFDM incumbent devices. We first reminded that in these scenarios, interference between users with different physical layers is usually measured according to the PSD of the interfering signal. This PSD-based model, though practical, only encompasses the effects of interference in the channel, at the input antenna of the receiver that suffers from interference.

However, interference should actually be measured based on EVM after the demodulation operations, before the constellation decoding. We therefore compared values of interference measured at this stage with those predicted by the PSD-based model. We showed that there is a tremendous gap between the PSD-based and EVM-based model, and went on to explain that this is due to the fact that the CP-OFDM receiver truncates the incoming interfering signal, which destroys the advantageous PSD properties of FB-MC signals. We further validated these results through mathematical analysis and experimentation. The obtained results show that secondary users based on FB-MC waveforms interfere on CP-OFDM incumbent users in a similar extent as CP-OFDM based secondary users. Though the mathematical and analytical considerations behind this work are not particularly complex, they had been totally omitted in a vast majority of the works available in the literature.

Finally, the study carried out in this article shows that the in-band coexistence of new 5G communications with legacy systems will only marginally be improved through the use of FB-MC waveforms. This improvement would be even more limited if signal impairments caused by the non-linear high power amplifier underlined for example in [38] came into play. Future work should therefore extend the presented analysis to take these impairments into account. Future studies should also focus on understanding how channel coding affects the presented results, an aspect that was left out of the scope of this article.

Nevertheless, based on the presented analysis, we can affirm that FB-MC does not efficiently reduce interference to CP-OFDM receivers. Other technologies that are currently being studied for 5G, such as the use of Massive MIMO, are therefore likely to be much more efficient at protecting incumbent legacy CP-OFDM users.

Appendix

Consider a rectangular window of length T, noted Π_T and a filter g of length T_g. We assume that g respects the following properties: it is equal to 0 anywhere except for $t \in [a,\ a+T_g]$ and is Lebesgue integrable on its non null area. Note that this is not a strong assumption and that filters commonly used in the literature respect it. We also add the condition that $T_g > T$. Under these assumptions, it is possible to define g as a truncation of a periodic signal $g_\infty(t)$ defined as

$$g_\infty(t) = g(\frac{t-a}{T_g}), \forall t \in \mathbb{R}. \tag{41}$$

$$A_{\Pi_T,g}(\tau,\nu) = \begin{cases} 0, & \tau > T-a \text{ or } \tau < -(a+T_g). \\ (a+\tau+T_g)e^{j\pi\nu(a+\tau+T_g)} \sum\limits_{k\in\mathbb{Z}} G_k e^{j\pi\frac{k}{T_g}(a-\tau+T_g)} \text{sinc}(\pi(\frac{k}{T_g}+\nu)(a+\tau+T_g)), & -(a+T_g) \le \tau \le T-(a+T_g) \\ (T-(a+\tau))e^{j\pi\nu(a+\tau+T)} \sum\limits_{k\in\mathbb{Z}} G_k e^{j\pi\frac{k}{T_g}(a-\tau+T)} \text{sinc}(\pi(\frac{k}{T_g}+\nu)(T-(a+\tau))), & -a \le \tau \le T-a \\ Te^{j\pi\nu T} \sum\limits_{k\in\mathbb{Z}} G_k e^{j\pi\frac{k}{T_g}(T-2\tau)} \text{sinc}(\pi(\frac{k}{T_g}+\nu)T), & T-(a+T_g) \le \tau \le -a \end{cases} \quad (51)$$

With this definition, $g_\infty(t)$ is a T_g-periodic signal which is Lebesgue integral on one period. Therefore, it can be decomposed in Fourier series as

$$g_\infty(t) = \sum_{k\in\mathbb{Z}} G_k e^{j2\pi k\frac{t}{T_g}}, t \in \mathbb{R}, \quad (42)$$

where G_k are the Fourier coefficients of $\tilde{g}$. Therefore, the cross-ambiguity function of g and a rectangular window of length T is equal to

$$A_{\Pi_T,g}(\tau,\nu) = \int_0^T g(t-\tau)e^{j2\pi t\nu}dt, \quad (43)$$

$$= \sum_{k\in\mathbb{Z}} G_k e^{-j2\pi k\frac{\tau}{T_g}} \int_0^T e^{j2\pi t(\frac{k}{T_g}+\nu)}dt, \quad (44)$$

which simplifies into different expressions according to the values of τ. Note that here, we consider that $T_g \ge T$.

Case I: $\tau > T-a$ or $\tau < -(a+T_g)$.

In that case, $g(t-\tau)$ does not overlap the rectangular window and

$$A_{\Pi_T,g}(\tau,\nu) = 0 \quad (45)$$

Case II: $-(a+T_g) \le \tau \le T-(a+T_g)$

In that case, only a small part of the filter overlaps the beginning of the rectangular window and

$$A_{\Pi_T,g}(\tau,\nu) = \sum_{k\in\mathbb{Z}} G_k e^{-j2\pi k\frac{\tau}{T_g}} \int_0^{a+\tau+T_g} e^{j2\pi t(\frac{k}{T_g}+\nu)}dt \quad (46)$$

Case III: $-a \le \tau \le T-a$

In that case, only a small part of the filter overlaps the end of the rectangular window and

$$A_{\Pi_T,g}(\tau,\nu) = \sum_{k\in\mathbb{Z}} G_k e^{-j2\pi k\frac{\tau}{T_g}} \int_{a+\tau}^T e^{j2\pi t(\frac{k}{T_g}+\nu)}dt \quad (47)$$

Case IV: $T-(a+T_g) \le \tau \le -a$

In that case, the filter g overlaps with the whole rectangular window and

$$A_{\Pi_T,g}(\tau,\nu) = \sum_{k\in\mathbb{Z}} G_k e^{-j2\pi k\frac{\tau}{T_g}} \int_0^T e^{j2\pi t(\frac{k}{T_g}+\nu)}dt \quad (48)$$

In order to give a simplified expression of $A_{\Pi_T,g}(\tau,\nu)$ in all the listed cases, we derive in the following lines the generic expression of $I_b^c = \int_b^c e^{j2\pi t(\frac{k}{T_g}+\nu)}$.

$$I_b^c = \frac{e^{j2\pi c(\frac{k}{T_g}+\nu)} - e^{j2\pi b(\frac{k}{T_g}+\nu)}}{j2\pi(\frac{k}{T_g}+\nu)} \quad (49)$$

$$= (c-b)e^{j\pi(\frac{k}{T_g}+\nu)(b+c)} \text{sinc}\left(\pi(\frac{k}{T_g}+\nu)(c-b)\right). \quad (50)$$

Putting (50) into (45) − (48), we obtain the expression of (51), as shown at the top of this page, for $A_{\Pi_T,g}(\tau,\nu)$.

REFERENCES

[1] J. G. Andrews *et al.*, "What will 5G be?" *IEEE J. Sel. Areas Commun.*, vol. 32, no. 6, pp. 1065–1082, Jun. 2014.

[2] G. Wunder and I. S. Gaspar, "5GNOW—5G cellular communications scenarios and system requirements," 5GNOW Project Consortium, Germany, Tech. Rep. D2.1, 2013.

[3] P. Banelli, S. Buzzi, G. Colavolpe, A. Modenini, F. Rusek, and A. Ugolini, "Modulation formats and waveforms for 5G networks: Who will be the heir of OFDM?: An overview of alternative modulation schemes for improved spectral efficiency," *IEEE Signal Process. Mag.*, vol. 31, no. 6, pp. 80–93, Nov. 2014.

[4] S. Haykin, "Cognitive radio: Brain-empowered wireless communications," *IEEE J. Sel. Areas Commun.*, vol. 23, no. 2, pp. 201–220, Feb. 2005.

[5] J. Mitola, "Cognitive radio: An integrated agent architecture for software defined radio," Ph.D. dissertation, Dept. Teleinformatics, Royal Inst. Technol. (KTH), Sweden, 2000.

[6] T. A. Weiss and F. K. Jondral, "Spectrum pooling: An innovative strategy for the enhancement of spectrum efficiency," *IEEE Commun. Mag.*, vol. 42, no. 3, pp. S8–14, Mar. 2004.

[7] M. Shaat and F. Bader, "Computationally efficient power allocation algorithm in multicarrier-based cognitive radio networks: OFDM and FBMC systems," *EURASIP J. Adv. Signal Process.*, 2010, Art. no. 5.

[8] H. A. Mahmoud, T. Yucek, and H. Arslan, "OFDM for cognitive radio: Merits and challenges," *IEEE Wireless Commun.*, vol. 16, no. 2, pp. 6–15, Apr. 2009.

[9] J. Abdoli, M. Jia, and J. Ma, "Filtered OFDM: A new waveform for future wireless systems," in *Proc. IEEE 16th Int. Workshop Signal Process. Adv. Wireless Commun. (SPAWC)*, Jun. 2015, pp. 66–70.

[10] T. Wild, F. Schaich, and Y. Chen, "5G air interface design based on universal filtered (UF-)OFDM," in *Proc. 19th Int. Conf. Digit. Signal Process.*, Aug. 2014, pp. 699–704.

[11] A. M. Tonello, "Performance limits for filtered multitone modulation in fading channels," *IEEE Trans. Wireless Commun.*, vol. 4, no. 5, pp. 2121–2135, Sep. 2005.

[12] M. Renfors *et al.*, "D2.1: FB-MC and enhanced OFDM schemes," Project ICT-Emphatic, Finland, Tech. Rep. D2.1, 2013.

[13] P. Siohan, C. Siclet, and N. Lacaille, "Analysis and design of OFDM/OQAM systems based on filterbank theory," *IEEE Trans. Signal Process.*, vol. 50, no. 5, pp. 1170–1183, May 2002.

[14] B. Farhang-Boroujeny, "OFDM versus filter bank multicarrier," *IEEE Signal Process. Mag.*, vol. 28, no. 3, pp. 92–112, May 2011.

[15] M. Bellanger, D. Mattera, and M. Tanda, "A filter bank multicarrier scheme running at symbol rate for future wireless systems," in *Proc. Wireless Telecommun. Symp.*, Apr. 2015, pp. 1–5.

[16] G. Fettweis, M. Krondorf, and S. Bittner, "GFDM—Generalized frequency division multiplexing," in *Proc. IEEE 69th Veh. Technol. Conf. (VTC)*, Apr. 2009, pp. 1–4.
[17] N. Michailow *et al.*, "Generalized frequency division multiplexing for 5th generation cellular networks," *IEEE Trans. Commun.*, vol. 62, no. 9, pp. 3045–3061, Sep. 2014.
[18] H. Lin and P. Siohan, "Multi-carrier modulation analysis and WCP-COQAM proposal," *EURASIP J. Adv. Signal Process.*, vol. 2014, no. 1, p. 79, 2014.
[19] D. Noguet, M. Gautier, and V. Berg, "Advances in opportunistic radio technologies for TVWS," *EURASIP J. Wireless Commun. Netw.*, vol. 2011, no. 1, pp. 1–12, 2011.
[20] A. Skrzypczak, J. Palicot, and P. Siohan, "OFDM/OQAM modulation for efficient dynamic spectrum access," *Int. J. Commun. Netw. Distrib. Syst.*, vol. 8, nos. 3–4, pp. 247–266, 2012.
[21] Y. Huang, B. Su, and I.-K. Fu, "Heterogeneous LTE downlink spectrum access using embedded-GFDM," in *Proc. IEEE Int. Conf. Commun. Workshops (ICC)*, May 2016, pp. 474–479.
[22] N. Michailow, M. Lentmaier, P. Rost, and G. Fettweis, "Integration of a GFDM secondary system in an OFDM primary system," in *Proc. Future Netw. Mobile Summit*, Jun. 2011, pp. 1–8.
[23] G. Jue and S. Shin, "Implementing a flexible testbed for 5G waveform generation and analysis—White paper," Keysight Technologies, Santa Rosa, CA, USA, Tech. Rep., Apr. 2015.
[24] F. Kaltenberger, R. Knopp, M. Danneberg, and A. Festag, "Experimental analysis and simulative validation of dynamic spectrum access for coexistence of 4G and future 5G systems," in *Proc. Eur. Conf. Netw. Commun. (EuCNC)*, Jun. 2015, pp. 497–501.
[25] F. Kaltenberger, R. Knopp, C. Vitiello, M. Danneberg, and A. Festag, "Experimental analysis of 5G candidate waveforms and their coexistence with 4G systems," in *Proc. Joint NEWCOM/COST Workshop Wireless Commun. (JNCW)*, Barcelona, Spain, Oct. 2015, pp. 1–4.
[26] V. Berg, J.-B. Doré, and D. Noguet, "A flexible radio transceiver for TVWS based on FBMC," *Microprocessors Microsyst.*, vol. 38, no. 8, pp. 743–753, Nov. 2014.
[27] Y. Medjahdi, M. Terré, D. L. Ruyet, and D. Roviras, "Interference tables: A useful model for interference analysis in asynchronous multicarrier transmission," *EURASIP J. Adv. Signal Process.*, vol. 2014, no. 54, pp. 1–17, 2014.
[28] R. Ahmed, T. Wild, and F. Schaich, "Coexistence of UF-OFDM and CP-OFDM," in *Proc. IEEE 83rd Veh. Technol. Conf. (VTC)*, May 2016, pp. 1–5.
[29] Q. Bodinier, A. Farhang, F. Bader, H. Ahmadi, J. Palicot, and L. A. DaSilva, "5G waveforms for overlay D2D communications: Effects of time-frequency misalignment," in *Proc. IEEE Int. Conf. Commun. (ICC)*, Kuala Lumpur, Malaysia, May 2016, pp. 1–7.
[30] Q. Bodinier, F. Bader, and J. Palicot, "Modeling interference between OFDM/OQAM and CP-OFDM: Limitations of the PSD-based model," in *Proc. 23rd Int. Conf. Telecommun. (ICT)*, Thessaloniki, Greece, May 2016, pp. 1–7.
[31] Q. Bodinier, F. Bader, and J. Palicot, "Coexistence in 5G: Analysis of cross-interference between OFDM/OQAM and legacy users," in *Proc. IEEE Globecom Workshops (GC Wkshps)*, Dec. 2016, pp. 1–6.
[32] J. Wang *et al.*, "Nonlinear inter-band subcarrier intermodulations of multi-RAT OFDM wireless services in 5G heterogeneous mobile fronthaul networks," *J. Lightw. Technol.*, vol. 34, no. 17, pp. 4089–4103, Sep. 1, 2016.
[33] H. Xing and M. Renfors, "Investigation of filter bank based device-to-device communication integrated into OFDMA cellular system," in *Proc. 11th Int. Symp. Wireless Commun. Syst. (ISWCS)*, Aug. 2014, pp. 513–518.
[34] C. Sexton, Q. Bodinier, A. Farhang, N. Marchetti, F. Bader, and L. A. DaSilva, "Coexistence of OFDM and FBMC for underlay D2D communication in 5G networks," in *Proc. IEEE Globecom Workshops (GC Wkshps)*, Dec. 2016, pp. 1–7.
[35] *FCC Second Memorandum Opinion and Order in the Matter of Unlicensed Operation in the TV Broadcast Bands*, Federal Communications Commission, Washington, DC, USA, 2010.
[36] D. R. I. Brown and A. G. Kelin, "Synchronization concepts," in *Coordinated Multi-Point in Mobile Communications: From Theory to Practice*, P. Marsch and G. P. Fettweis, Eds. Cambridge, U.K.: Cambridge Univ. Press, 2011, ch. 8.1, pp. 161–170.
[37] M. G. Bellanger, "Specification and design of a prototype filter for filter bank based multicarrier transmission," in *Proc. IEEE Int. Conf. Acoust., Speech, Signal Process.*, vol. 4, May 2001, pp. 2417–2420.
[38] M. Renfors, J. Yli-Kaakinen, and M. Valkama, "Power amplifier effects on frequency localized 5G candidate waveforms," in *Proc. 22nd Eur. Wireless Conf.*, May 2016, pp. 1–5.

QUENTIN BODINIER received the Engineering degree and the M.Sc. degree in wireless communications, embedded electronics, and networks from CentraleSupélec, Rennes, France, in 2014, where he is currently pursuing the Ph.D. degree in wireless communications for 5G with the SCEE Research Team. His research activities focus on studying how new physical layer technologies, such as advanced multicarrier waveforms, can enhance the coexistence of 5G communications, such as D2D, M2M, or Internet of Things, with legacy LTE networks. More broadly, he has a strong interest in techniques that bring flexibility and cognitive capabilities to wireless networks. He has been involved in the Newcom# European project and the ACCENT5 National Project. He received the PhC. ULYSSES grant for cooperating with Ireland in 2015, the 2015 Newcom# mobility grant, and the IEEE ICC 2016 Student Travel Grant.

FAOUZI BADER (SM'07) received the Ph.D. degree (Hons.) in telecommunications from the Universidad Politécnica de Madrid, Madrid, Spain, in 2002. He joined the Center Technologic de Telecomunicacions de Catalunya, Barcelona, Spain, as an Associate Researcher in 2002, where he was nominated as a Senior Research Associate in 2006. Since 2013, he has been an Associate Professor with CentraleSupélec, Rennes, France. His research activities mainly focus on advanced multicarrier waveforms (OFDM(A), (non-) uniform multimode filter-based multicarrier schemes) and frequency allocation techniques in relay cognitive environments. He has been involved in several European projects from the 5th–7th EC research frameworks, and from 2012 to 2013, he was nominated as the General Coordinator and the Manager of the EC-funded research project ICT EMPhAtiC, focusing on enhanced multicarrier techniques for professional ad-hoc and cell-based communications. He has authored more than 120 papers in peer-reviewed journals and international conferences, more than 13 book chapters, and published three books. He served as Technical Program Committee Member in major IEEE ComSoc and VTS conferences, and as the General Chair of the eleventh edition of the ISWCS'2014 conference, and the Co-Chair of the ISWCS 2015 edition.

JACQUES PALICOT received the Ph.D. degree in signal processing from the University of Rennes, France, in 1983.

Since 1988, he has been involved in studies about equalization techniques applied to digital transmissions and analog TV systems. Since 1991, he has been involved mainly in studies concerning the digital communications area and automatic measurements techniques. From 2001 to 2003, he had a temporary position with INRIA/IRISA, Rennes. Since 2003, he has been with CentraleSupélec, Rennes, where he leads the Signal Communications and Embedded Electronics Research Team. He has taken an active part in various international bodies, such as EBU, CCIR, URSI, and within RACE, ACTS, and IST European projects. He has authored various scientific articles, notably on equalization techniques, echo cancellation, hierarchical modulations, and software radio techniques. He is author or co-author of more than 300 publications with more than 50 in journals, and two books. He holds 22 patents. He is currently involved in adaptive signal processing, digital communications, software radio, cognitive radio, and green radio.

Dr. Palicot has been an Associate Editor of the EURASIP JASP, since 2008. He also served as the Lead Guest Editor of several special issues on software radio, cognitive radio, and green radio. He was the Co-General Chairman of ISCIT 2011, Co-General Chairman of Next-GWiN 2014, and the Technical Program Chairman of the CROWNCOM 2009, the GREENCOM 2013, and CRN Symposium of ICC 2014.